Title: Simulations of Moisture Movement through Pits 37 and 38 at Los Alamos National Laboratory Technical Area 54, Area G

Author(s): Dai, Zhenxue
Birdsell, Kay Hanson
Stauffer, Philip H.
Newman, Brent David

Intended for: Report

Issued: 2018-05-21 (rev.1)

Simulations of Moisture Movement

Through

Pits 37 and 38 at

Los Alamos National Laboratory

Technical Area 54, Area G

Authors:
Zhenxue Dai, Kay Birdsell, Philip Stauffer, and Brent Newman
Los Alamos National Laboratory

1.0 Introduction

Los Alamos National Laboratory (LANL) uses the Area G disposal facility to dispose of the low-level radioactive waste at Technical Area 54 (TA-54). Figure 1-1 shows the locations of the disposal pits and shafts at Area G. Historically, pits have been filled with waste to within 0.6 to 3 m of the surface; the remaining space is filled with crushed tuff during interim closure (Levitt, 2011). Infiltration from precipitation may leach and transport the low-level radioactive waste from the pits and shafts downward to the regional aquifer beneath Area G. The work performed for this report builds on simulations of infiltration into Pits 37 and 38 performed by Levitt (2011), who determined the impact of adding significant volume of dust suppression water during the disposal of uncontainerized wastes removed from former Material Disposal Area B at TA-21, to consider the impact of long-term precipitation into the pits. The software HYDRUS (1D, 2D and 3D) developed by Šimůnek et al. (2011) is used for the simulations. For the study, the model is calibrated to the variably-unsaturated conditions in Area G, and is applied for estimating the infiltration rates through the waste and fill in the pits to calculate transient water flux out the bottoms of disposal pits to the underlying rocks. The water flux is, in turn, used for groundwater pathway analyses conducted with FEHM (Zyvoloski et al., 2011) to further understand the mobility of radionuclides from the pit to the underlying regional aquifer (Pawar et al., 2018). The study builds on work presented in *Special Analysis 2012-007: Impacts of Water Introduced into Pits 37 and 38 at Technical Area 54, Area G* (French et al., 2013).

This effort addresses infiltration conditions of recent years; especially the large rainfall event that occurred in September 2013. The infiltration modeling effort described in this report considers the rates of water movement through the bottoms of the disposal pits as they receive waste, after interim closure, and following final closure. The observed precipitation data from January 1, 1990 to June 30, 2015 are used as inputs for the infiltration models, which updates previously used precipitation inputs by approximately 3 years and includes the large rainfall in September of 2013. Assumptions regarding infiltration through the waste are also updated based on operations. Recent monitoring data (as well as some previous monitoring data) from Area G provide

volumetric water and hydraulic pressure profiles (Levitt et al., 2015), which are used to calibrate the flow model parameters.
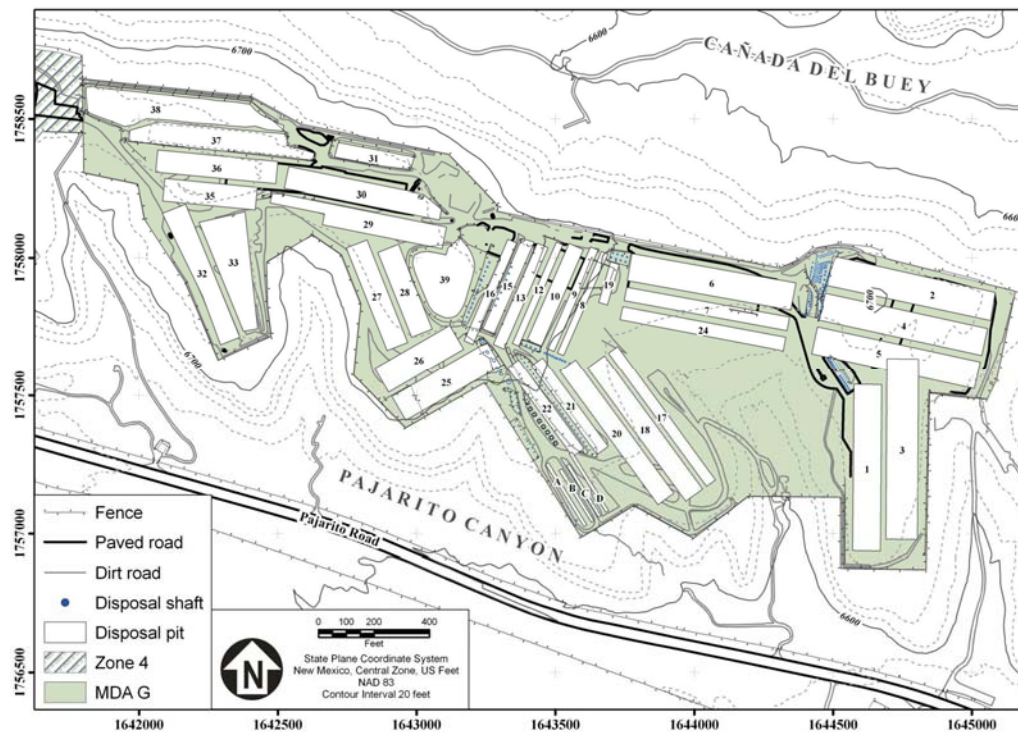

Figure 1-1: Waste disposal units at Area G (modified from Levitt et al., 2015)

Section 2 of this report presents the theory for water flow in the variably-saturated media, which is included in the software HYDRUS. Then we use the existing monitoring data to conduct flow model validation (in section 3). In section 4, we discuss the detailed infiltration models under various scenarios and compare the results with those of the previous studies. In this study we mainly used HYDRUS-2D for simulating the water flow in the unsaturated pits and the surrounding rocks with various different approaches.

2.0 Water flow model

The HYDRUS-2D flow models used in this study are based on geological framework models developed by Broxton and Vaniman (2005) and others. Figures 2-1 and 2-2 show a cross section consisting of eight geological units and their thicknesses in the vadose zone. Broxton and Vaniman (2005) and Springer (2005) provided an overview of the regional and site-specific

geological and hydrological conditions of the study area. The waste pits and boreholes plotted in Figure 2-3 occur mainly in subunits of the Tshirege Member of the Bandelier Tuff as shown in Figure 2-1. We assume that water flow in the variably saturated porous media is Darcian flow, and the flow equation is given by a modified form of the Richards' equation (Dai and Samper, 2004; Dai et al., 2008; Šimůnek et al., 2011):

$$\nabla \cdot (K_r K_s \nabla h) + w = (\varphi \frac{\partial S_w}{\partial \psi} + S_w S_s) \frac{\partial \psi}{\partial t},$$

(1)

where h is hydraulic head, which is the sum of pressure head ψ and elevation Z or $h = \psi + Z$.

Hydraulic conductivity K is the product of relative conductivity K_r and saturated conductivity K_s. S_w is water saturation degree defined as the ratio between volumetric water content θ and porosity ϕ, or $S_w = \theta / \phi$ (for fully saturated media $S_w = 1$). Water saturation is related to pressure head through retention curve $S_w(\psi) = S_r + (1 - S_r)[1 + (-\alpha \psi)^n]^{-m}$, where S_r is the residual water saturation and m, n and $\alpha(1 / L^{-1})$ are Van Genuchten parameters usually estimated by fitting this function to observation data (van Genuchten, 1980). S_s is the specific storage coefficient. The symbols $\nabla \cdot [\ ]$ and $\nabla (\ )$ are the divergence and gradient operators, respectively. w is a source or sink term, which include precipitation, evapotranspiration and plant (or root) water uptake, or the volume of water removed from a specific volume of soil in a specific time due to plant water uptake. Feddes model (1974) and van Genuchten approach (1987) are used to calculate the root water uptake.

The finite element numerical method combined with Newton-Raphson iteration scheme is used to solve the nonlinear equation numerically, and the algorithm is implemented in HYDRUS (Šimůnek and Hopmans 2009; Šimůnek et al., 2008; 2011).
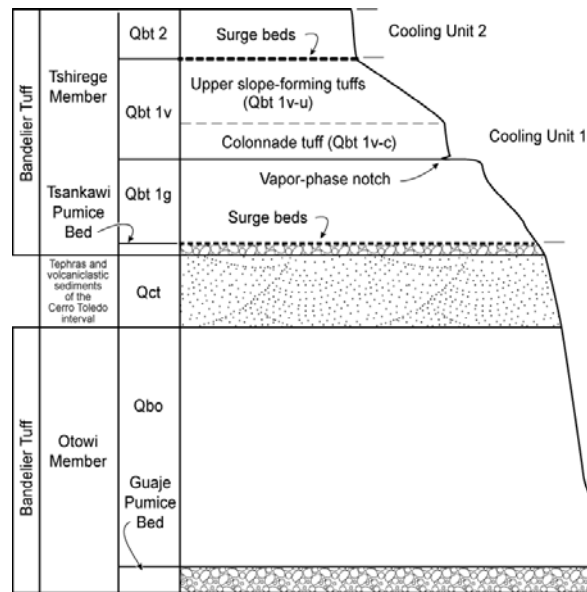
Figure 2-1: The stratigraphy of the Bandelier Tuff beneath Area G (Adapted from Broxton and Reneau, 1995)
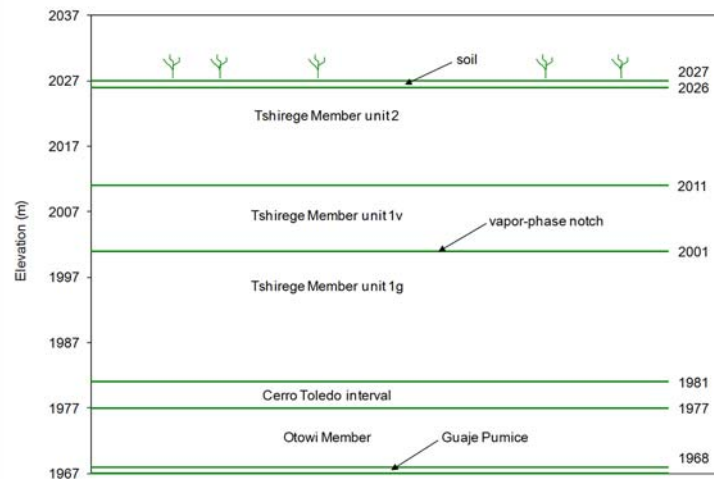

Figure 2-2: The Generalized stratigraphy of the Bandelier Tuff units beneath Area G and their thicknesses which are used in this study (Adapted from Levitt, 2011)
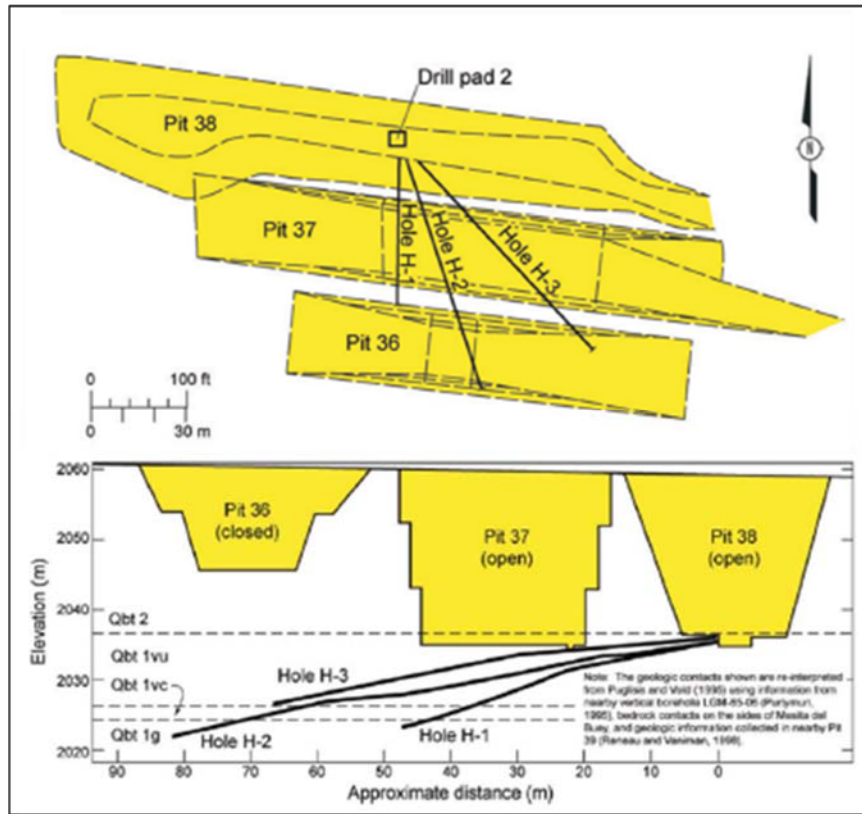
Figure 2-3: Plan view (top) and profile view (bottom) of boreholes H-1, H-2, H-3 drilled under Pits 38, 37 and 36 (from McLin et al., 2005).

3.0 Model validation with monitoring data

Since the 1980s, periodic monitoring has been conducted in the unsaturated zone at Area G. Several sets of horizontal and vertical boreholes were installed for monitoring of water content below and within waste pits (Levitt et al., 2015). The following three sub-sections discuss model validation using these monitoring data.

3.1. Water contents beneath Pits 36, 37, and 38

The first set of monitoring data was observed from a set of three near-horizontal boreholes located at the bottom of Pit 38 that extended beneath Pits 37 and 36 (see Figure 2-3). Pit 36 was excavated in 1988 and capped in 1996, while Pit 37 was excavated in 1990 and capped in 2000. Pit 38 was excavated in 1994 and is not yet fully capped. Based on the spatial configuration of the three pits, we built a two-dimensional conceptual model as shown in Figure 3-1. The model parameters corresponding to each unit are adopted from Levitt (2011) and listed in Table 3-1.

5

Because we do not know the initial conditions of the subsurface rock within the mesa in 1988, we use an average infiltration rate (0.1 mm per year adopted from Levitt (2011)) and run the model for 1000 years to reach a steady state (Figure 3-2). We then use the computed hydraulic pressure distributions as our model initial condition to run the model from January 1, 1988 to 1995. In 1995, Pit 37 was active and had been receiving waste for about 5.5 years (the waste had a depth of 10 m), and Pit 38 was excavated and had just started to receive waste in the western end. The final water content distributions along the hole H-2 are plotted in Figure 3-3. The comparison between simulated and observed water contents (Figure 3-4) shows that our model results generally match the observations reasonably well.
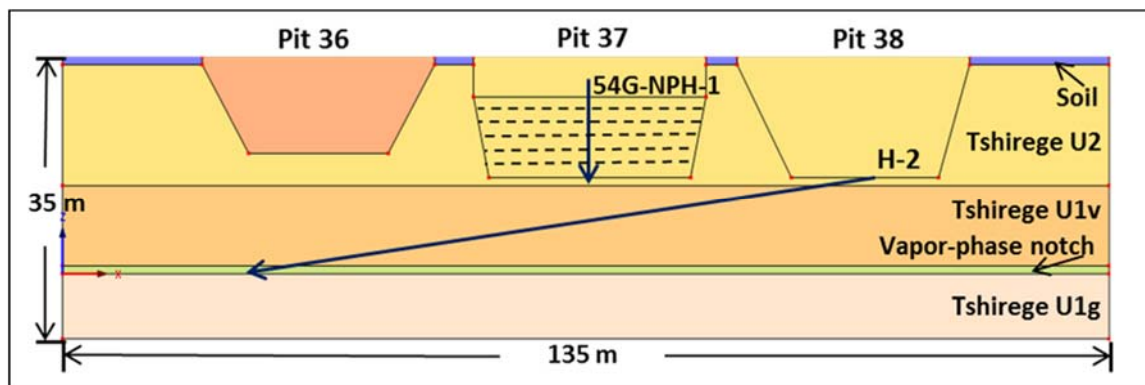

Figure 3-1: The conceptual model for simulating water contents beneath Pits 36, 37 and 38.

Table 3-1: Physical and chemical properties of materials and geological units*

Materials and units	Volumetric Water Content		van Genuchten Parameters		Saturated Conductivity (m/day)	Sources
	Residual	Saturated	α (1/m)	n		
Final Cover Material: crushed tuff + 6% bentonite	0.004	0.4	0.088	3.0	0.0016	Levitt (2008)
Soil	0.025 [a]	0.41	1.3	1.2	0.41[b]	Stauffer et al. (2005)
Crushed Tuff	0.01	0.33	1.3	1.5	0.25	Levitt (2008)
Crushed Tuff Cover	0.001	0.01	1.3	1.5	20.0	Birdsell (2000)
Waste	0.01	0.3 or 0.4	1.43	1.5	0.25	Levitt (2008)
Packaged Waste	0.0	0.001	1.43	1.5	0.00001	Estimated
Tshirege Member Unit 2	0.024	0.41	0.47	2.1	0.17 [c]	Stauffer et al. (2005)
Tshirege Member Unit 1v	0.006	0.49	0.36	1.7	0.1 [c]	
Vapor-phase Notch	0.0048	0.5	0.44	1.4	0.06	Vold (1997)
Tshirege Member Unit 1g	0.022	0.46	0.5	1.8	0.13 [c]	Stauffer et al. (2005)
Cerro Toledo Interval	0.007	0.45	1.3	1.5	0.15 [c]	
Otowi Member	0.043	0.44	0.59	1.8	0.2 [c]	
Guaje Pumice Bed	0.0	0.67	0.08	4.0	0.13 [c]	

[a] *Increased from value of 0.0 in Table III-1, Stauffer et al. (2005) to reflect more realistic value*

[b] *Ksat value was multiplied by 100 compared to source; see text for discussion*

[c] *Calculated from permeability value;* [d] *personal communication (October 8, 2015)*
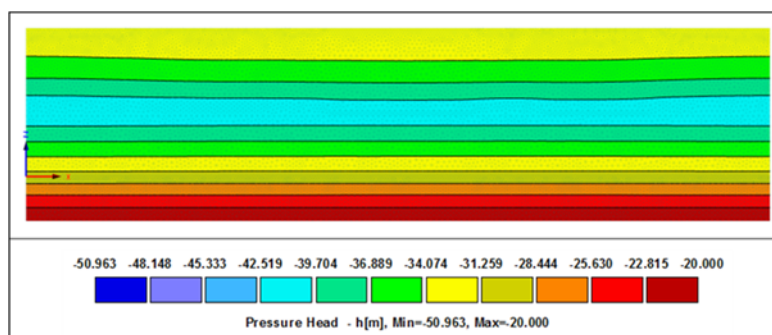
*Modified from Levitt (2011)

Figure 3-2: The simulated initial hydraulic pressure distributions beneath Pits 36, 37 and 38.
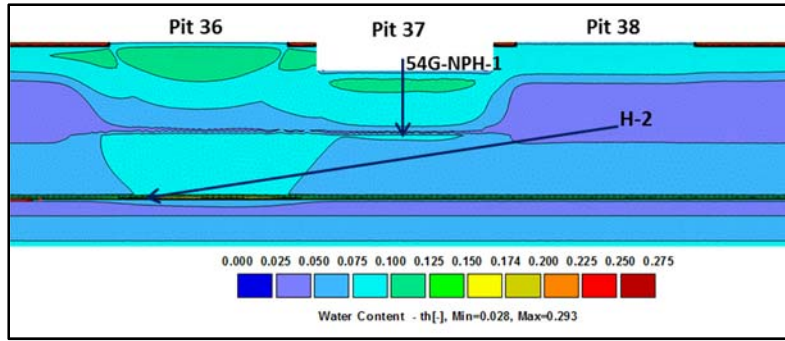
Figure 3-3: The simulated water content distributions beneath Pits 36, 37 and 38 in 1994 corresponding to the observed water contents in the horizontal hole H-2.
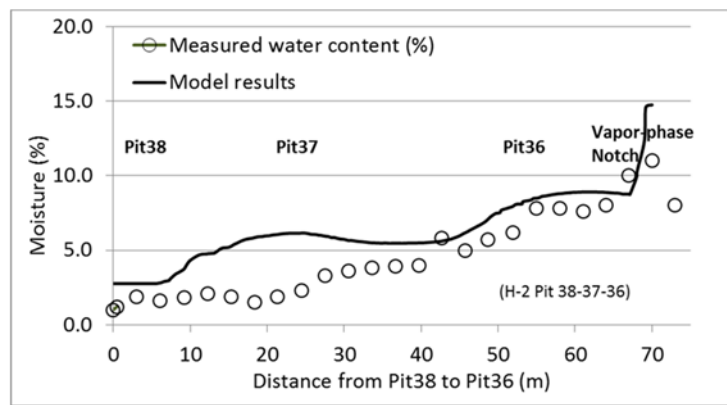

Figure 3-4: The comparison of the simulated and measured water contents beneath Pits 36, 37 and 38 in the horizontal hole H-2.

3.2. Water contents in boreholes 54G-NPH-1, 2 and 3

The second set of monitoring data was observed from a set of vertical boreholes located inside Pit 37 (western end; 54G-NPH-1), outside of Pit 37 (northeast corner; 54G-NPH-2), and north of Pit 30 (54G-NPH-3) (Loiza and Vold, 1995). Different two-dimensional models were built for simulating the vertical water content distributions for each of the three boreholes, respectively. Figure 3-5 shows the comparison of the simulated water contents within Pit 37 downward vertically from 0 to 10 m (which was the thickness of the filled waste) and the corresponding measured water contents in borehole 54G-NPH-1. The curve fitting results for boreholes 54G-NPH-2 and 54G-NPH-3 are shown in Figures 3-6 and 3-7. While model results for 54G-NPH-1 miss the peak of soil moisture observations, the overall results indicate that our numerical models can approximate the major observation data and the data trends, especially for 54G-NPH-2 and -3.
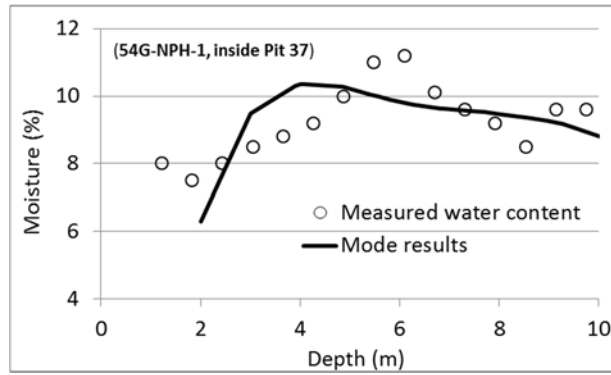
8

Figure 3-5: The comparison of the simulated and measured water contents within Pit 37 in borehole 54G-NPH-1.
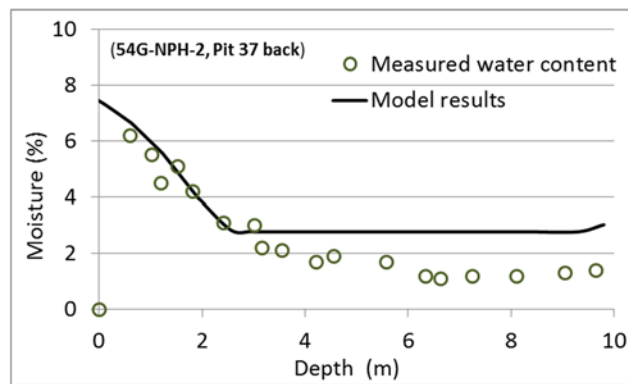

Figure 3-6: The comparison of the simulated and measured water contents in borehole 54G-NPH-2 (in the back of Pit 37).
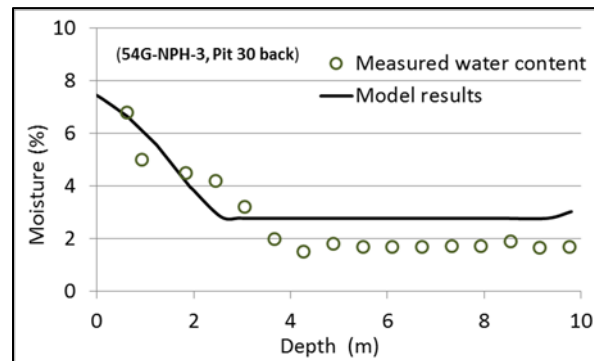

Figure 3-7: The comparison of the simulated and measured water contents in borehole 54G-NPH-3 (in the back of Pit 30).

9

3.3. Matric potential measurements in Pit 38 Extension

The third set of the measurements were obtained from three shallow boreholes (BH54-1, BH54-2 and BH54-3) located in the Pit 38 Extension, as shown in Figure 3-8. By using the 2-D model built for the Pit 38 Extension simulations (*stage a*, see Sections 4.1 and 4.2 for the stage definition), we calculate the transient matric potential (hydraulic pressure) in these three boreholes at different depths. For matching the observations at different depths, we used very fine numerical grids at the bottom of the Pit 38 Extension (Figure 3-9). The 2-D model was first run with a constant infiltration rate of 0.1 mm/year on the top of the model to reach a steady state, and then the steady-state pressure distribution was used as the initial condition for model validation (Figure 3-10). The precipitation data from July 1, 2012 to February 24, 2015 are shown in Figure 3-11. Matric potential measurements from boreholes BH54-1, BH54-2 and BH54-3 at the bottom of Pit 38 Extension are used for model validation during 2012-2015 (Levitt et al., 2015).

Simulated results and measured data from July 1, 2012 to February 24, 2015 are plotted in Figure 3-12. Our modeling results are closer to the mean of the observation curve of BH54-3, but the observed potentials from three different locations below the pit bottom have a larger variation than our model results. It is likely that discrepancies between the observed and simulated potentials are due to simplified representation of rock layers beneath the pit. We assumed a uniform rock layer beneath the pit bottom for the Tshirege Member Unit 2 with a thickness of 15 m and a uniform distribution for water added to the bottom of the pit. In reality, the Unit 2 rocks are heterogeneous, and we would expect that precipitation infiltrates non-uniformly because of the ramp and small depressions in the pit floor, as illustrated in the photo in Figure 44 of Levitt et al., (2015). Another difference is that the van Genuchten parameters used to simulate matrix potential in the model (Table 3-1) may differ from the actual field conditions. However, our model mimics the major trends of the variations in matric potential at different depths, especially for the big storm that occurred in September of 2013. The potential increase after the storm is clear, and our model is even more sensitive to the storm than the observation data indicate. These results demonstrate that our model and the parameters can approximately reflect the hydrological and geological conditions reasonably well, which can be used for simulating the pit activities and predicting the water flow out of the pit bottom.
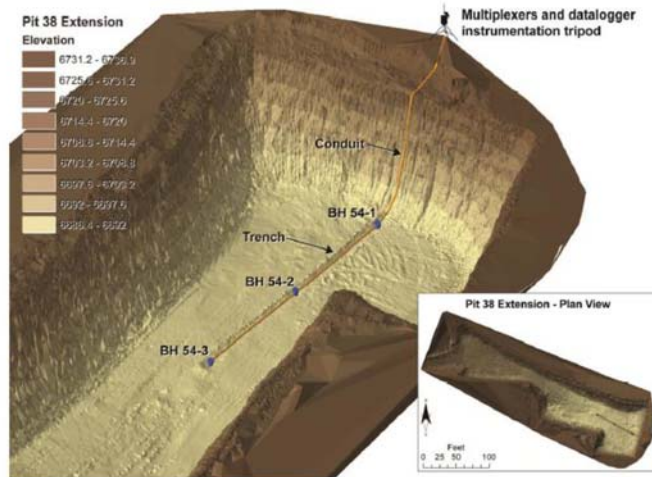
Figure 3-8: The location of boreholes BH54-1, BH54-2 and BH54-3 in the bottom of the Pit 38 extension (adopted from Levitt et al., 2015).
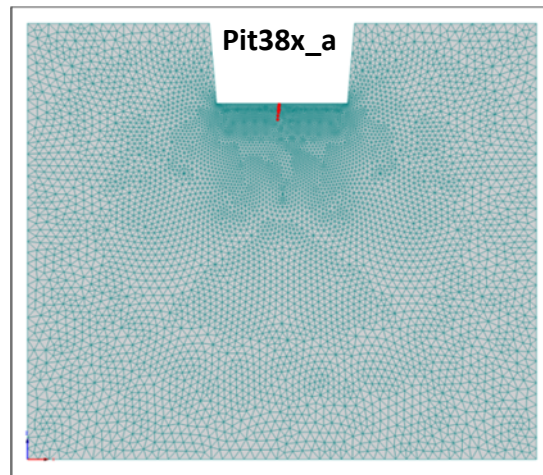

Figure 3-9: A two-dimensional numerical model for simulating water flow in the Pit 38 Extension. The model has a size of 70×60 m^2. The pit size is 11 m deep, 20 m wide on the top and 18 m at the bottom. The red dots (right below the pit bottom) are observation points that are used to match with the monitoring data for model validation.
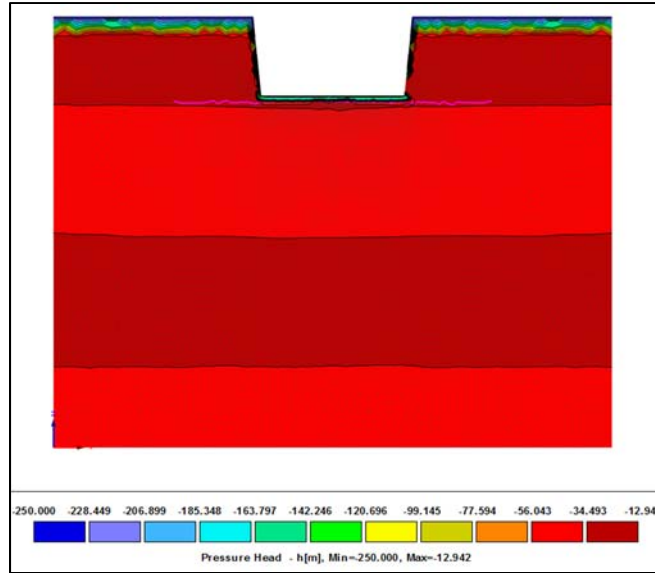
Figure 3-10: The initial hydraulic pressure (corresponding to matric potential) distribution obtained by running the model with a constant infiltration rate of 0.1 mm/year on the top to reach a steady state
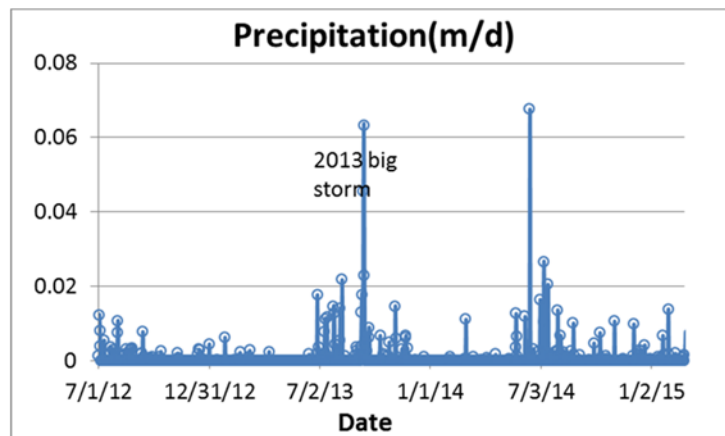

Figure 3-11: Precipitation data from July 1, 2012 to February 24, 2015, the time period corresponding to the measured matric potential data (Levitt et al., 2015)
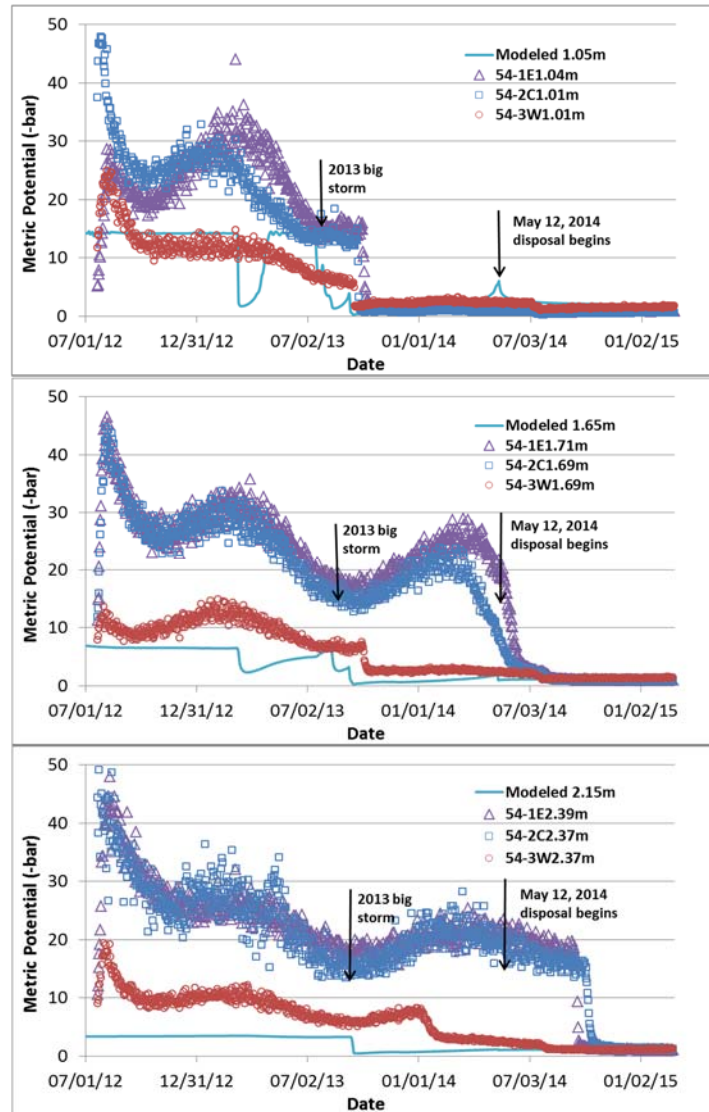
Figure 3-12: Comparison of modeled and observed potential (-bar) in *stage a* of Pit 38 extension.

4.0 Infiltration Models for Pits 37 and 38

In this section, we discuss the detailed infiltration models for Pits 37 and 38 (East, West, and Extension) using several scenarios. The transient infiltration rates through the bottom of the Pits are computed as the input for FEHM (Zyvoloski et al., 2010) calculations of groundwater flow and transport to the regional aquifer (Pawar et al., 2018).

4.1 Simulations for Pit 37

A two-dimensional cross section model is built for simulating water flow in Pit 37 with two scenarios. Five stages are used for each scenario based on the progression of waste disposal in Pit 37. A waste layer is assumed to be composed of both waste and fill (i.e., crushed tuff).

Scenario 1 (Pit37_1)

Stage a: January 1, 1990 to Dec. 31, 1993, 10-m-thick waste layer added to the bottom of the pit with initial saturation of 20%. Outside of the pit the initial hydraulic pressure of -70 m was assumed.

Stage b: January 1, 1994 to Dec. 31, 2007, 2-m-thick additional waste layer added to the pit with initial saturation of 20%.

Stage c: January 1, 2008 to December 31, 2012, 2-meter-thick additional waste layer added to the pit with initial saturation of 20%. Contaminant control water (decontamination water, 1332 m^3, during January 2011 to May 2011) was input to the top of the waste on a representative day (2/21/2011) to represent water added during MDA B waste disposal (see French et al. (2013)).

Stage d: January 1, 2013 to December 31, 2046, 1-meter-thick additional waste layer was added to the pit with initial saturation of 20%. The observed precipitation data from January 1, 2013 to June 30, 2015 were input to the model, including the large rainfall event that occurred during September, 2013. From July 2015 to the end of 2046, we used the predicted daily precipitation (see Appendix A) and evaporation/transpiration (PE and PT) to cover the whole period for the simulation of this stage.

Stage e: January 1, 2047 to Dec. 31, 3046, Pit assumed to be covered and closed. One-thousand-year prediction was conducted with a constant effective infiltration rate of 0.1 mm/year on the top of the model.

Scenario 2 (Pit37_2)

Stage a: Jan. 1, 1990 to Dec. 31, 1993, 10-m-thick waste layer added to the bottom of the pit with initial saturation of 33%. Outside of the pit the initial hydraulic pressure of -70 m was assumed.

Stage b: Jan. 1, 1994 to Dec. 31, 2007, 2-m-thick additional waste layer added to the pit with initial saturation of 33%.

Stage c: January 1, 2008 to December 31, 2012, 2-m-thick additional waste layer added to the pit with initial saturation of 33%. Contaminant control water (dust suppression and decontamination water, 1332 m^3, during January 2011 to May 2011) was input to the top of the waste on a representative day (2/21/2011) to represent water added during MDA B waste disposal (see French et al. (2013)).

Stage d: January 1, 2013 to December 31, 2046, 1-meter-thick additional waste layer was added to the pit with initial saturation of 33%. The observed precipitation data from January 1, 2013 to June 30, 2015 were input to the model, including the large rainfall event that occurred during September, 2013. From July 2015 to the end of 2046, we used the predicted daily precipitation (see Appendix A) and evaporation/transpiration (PE and PT) to cover the whole period for the simulation of this stage.

Stage e: January 1, 2047 to Dec. 31, 3046, Pit assumed to be covered and closed. One-thousand-year prediction was conducted with a constant effective infiltration rate of 0.1 mm/year on the top of the model.

The major difference between these two scenarios is the initial saturation assumed for the waste/fill placed in the pit, which is uncertain. Scenarios 1 and 2 are assigned initial waste saturations of 20% and 33%, respectively, for *stages a* through *d*. During the five stages, we output the water flow rates from the bottom of Pit 37 for both scenarios, which are used as inputs for the 3-dimensional FEHM simulations in this area (Pawar et al., 2018).

4.1.1 *Stage a* simulations – Pit 37

By using the geological framework model and the corresponding parameters obtained from Levitt (2011; 2013), we built a 2-D model for *stage a* simulations (Figure 4-1). After running the model from January 1, 1990 to Dec. 31, 1993, we first compare our modeling results for the two scenarios. Figure 4-2 shows the final simulated pressure head (m) distributions at the end of *stage a* (Dec. 31, 1993) for the two scenarios. With larger initial saturation for the waste in scenario 2, the water infiltrates much deeper than in scenario 1, and the flow rate across the

15

bottom of Pit 37 is much larger for scenario 2 than for scenario 1. Figure 4-3 shows the computed water flow rates across the pit bottom for the two scenarios.
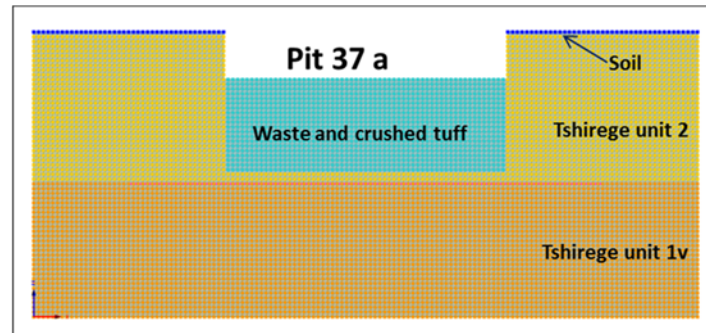

Figure 4-1: A two-dimensional numerical model for simulating water flow through Pit 37. A domain area of 70×30 m². The pit size is 15 m deep, 30 m wide on the top. The light blue area in the pit represents the waste layer (10-m-thick) emplaced during *stage a*, with initial saturations of 20% and 33% for the scenarios 1 and 2, respectively. The red line (right below the pit bottom) is an auxiliary mesh line for computing flow rate crossing the bottom of the pit.
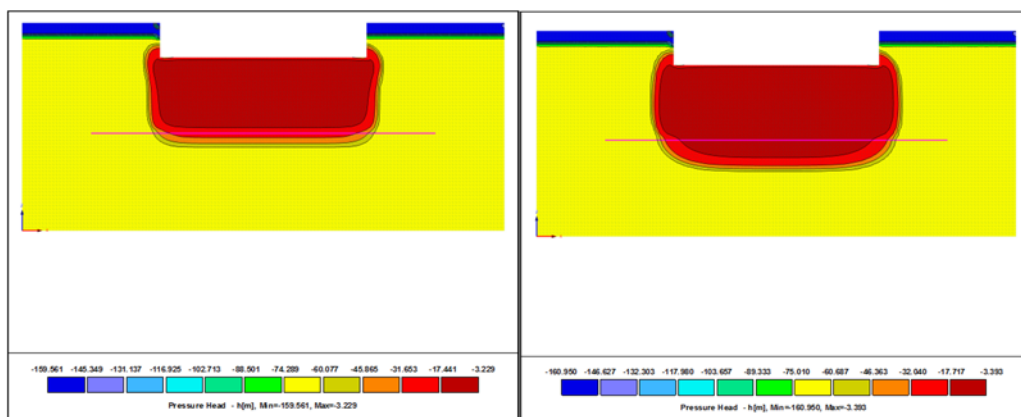

Figure 4-2: Simulated pressure head (m) distributions at the end of *stage a* (Dec. 31, 1993) for Pit 37 scenario 1 (left) and 2 (right)
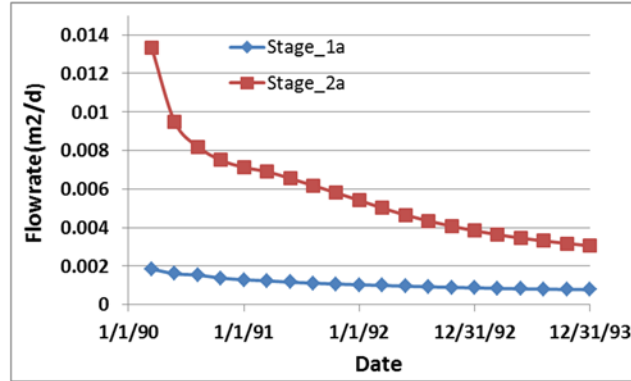
Figure 4-3: Computed water flow rates from the bottom of Pit 37 during *stage a* for scenarios 1 (blue) and 2 (red)

4.1.2 *Stage b* simulations – Pit 37

In *stage b,* we add a 2-meter-thick additional waste layer into Pit 37. The initial condition was input from the end results of *stage a* (Dec. 31, 1993, of the two scenarios), while the newly added waste has an initial saturation of 20% and 33% for the two scenarios, respectively. The simulated pressure head distributions at the end of *stage b* (Dec. 31, 2007) are shown in Figure 4-4. The computed water flow rates from the pit bottom are plotted in Figure 4-5. Scenario 2, with much larger initial saturation for the waste layer, has much more water flow across the bottom of Pit 37 at early time, and then the flow rates computed from the two scenarios become closer with time.
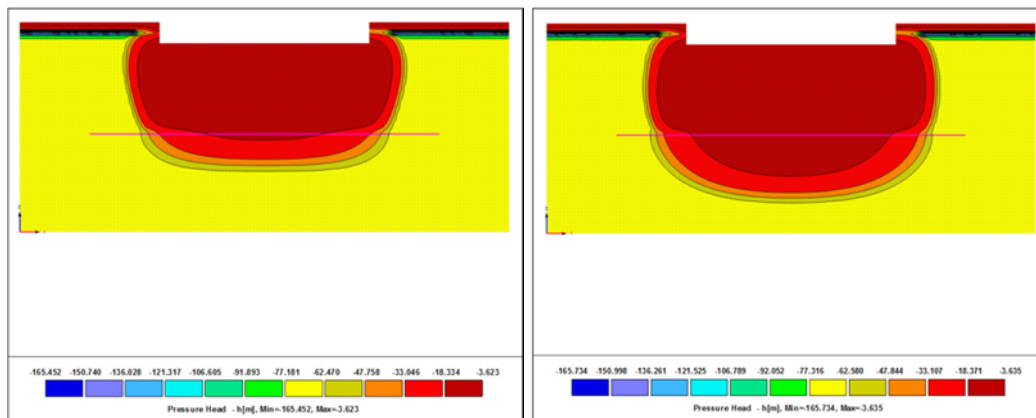

Figure 4-4: Simulated pressure head (m) distributions at the end of *stage b* (Dec. 31, 2007) for Pit 37 scenario 1 (left) and 2 (right).
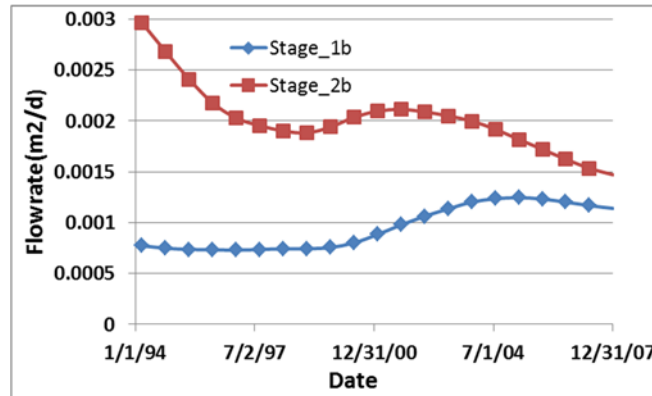
Figure 4-5: Computed water flow rates from the bottom of Pit 37 during *stage b* for scenarios 1 (blue) and 2 (red).

4.1.3 *Stage c* simulations – Pit 37

In *stage c,* we add a 2-meter-thick additional waste layer into Pit 37. The initial condition was input from the end results of the *stage b*, while the newly added waste has an initial saturation of 20% and 33% for the two scenarios, respectively. The simulated pressure head distributions at the end of *stage c* (Dec. 31, 2012) are shown in Figure 4-6. During this stage, the contaminant control water of 1332 m^3 (about 8000 gallon) was add to the top of the waste on a representative day March 21, 2011. The computed water flow rates from the pit bottom are plotted in Figure 4-7.
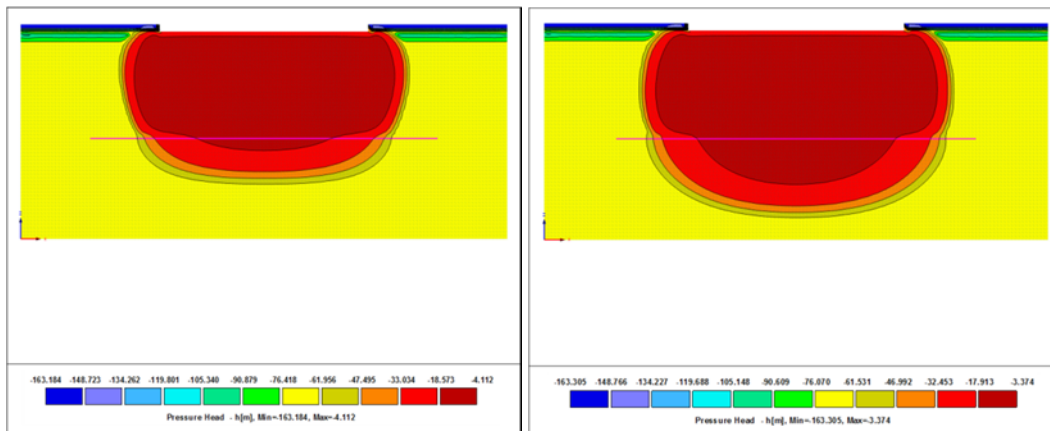

Figure 4-6: Simulated pressure head (m) distributions at the end of *stage c* (Dec. 31, 2012). The contaminant control water of 1332 m^3 (8000 gallon) was add to the top of the waste on March 21, 2011 for both Pit 37 scenario 1 (left) and 2 (right).
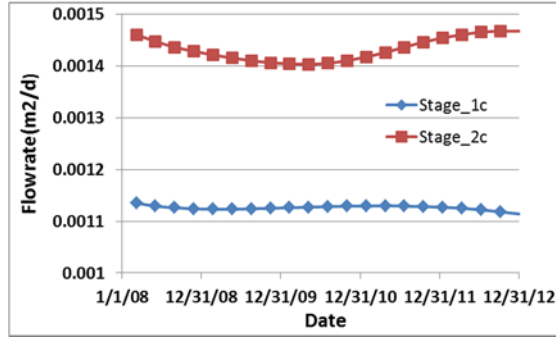
18

Figure 4-7: Computed water flow rates from the bottom of Pit 37 during *stage c* for scenarios 1 (blue) and 2 (red).

4.1.4 *Stage d* simulations – Pit 37

In *stage d,* we add an additional 1-m-thick waste layer on the top of the pit with initial saturation of 20% and 33% for the two scenarios, respectively. The end results (pressure distributions) of the *stage c* are used as the initial condition to run the model until December 31 of 2046. The observed precipitation data from January 1, 2013 to June 30, 2015 were input to the model, including the large multi-day rainfall in the fall of 2013. From July 2015 to end of 2046, we used predicted daily precipitation and evaporation/transpiration (PE and PT, Appendix A) to cover the remaining period for the simulation of this stage. The simulated pressure head distributions at the end of *stage d* (Dec. 31, 2046) are shown in Figure 4-8 for the two scenarios respectively. The computed water flow rates from the pit bottom are plotted in Figure 4-9, which shows that after 33 years, the flow rates across the bottom of Pit37 from both scenarios are similar. The difference of the initial waste layer saturations has a lasting impact on flow rates for about 50 years, at which point flow rates are governed by precipitation and infiltration conditions.
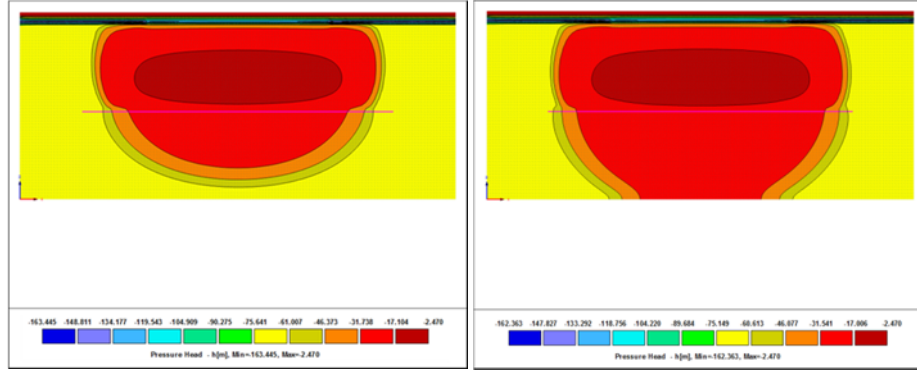
19

Figure 4-8: Simulated pressure head (m) distributions at the end of *stage d* (Dec. 31, 2046) for both Pit 37 scenarios 1 (left) and 2 (right).
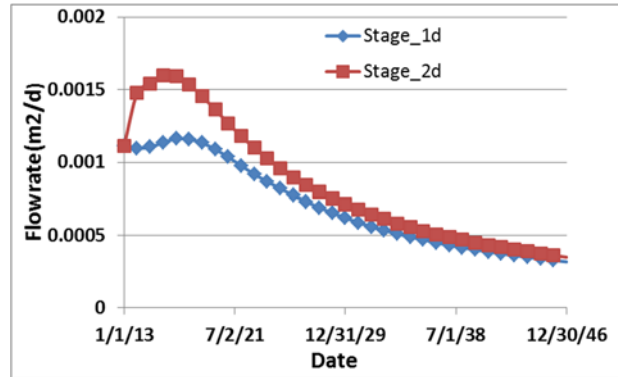

Figure 4-9: Computed water flow rates from the bottom of Pit 37 during *stage d* for scenarios 1 (blue) and 2 (red).

4.1.5 *Stage e* **simulations- Pit 37**

In *stage e,* we use the end results (pressure distributions) of *stage d* as an initial condition to run the model for one thousand years. An effective infiltration rate of 0.1 mm/year was added to the model top as a constant flow rate boundary. We also consider root uptake on the two sides external to the pit. The simulated water content and pressure head distributions at the end of *stage e* (Dec. 31, 3046) are shown in Figures 4-10 and 4-11, respectively. The computed water flow rates from the pit bottom are plotted in Figure 4-12. The computed flow rates for the two scenarios are nearly the same during this late time stage. The combined water flow rates from the pit bottom over the combined stages (*stage a to e*) are plotted in Figures 4-13 and 4-14.
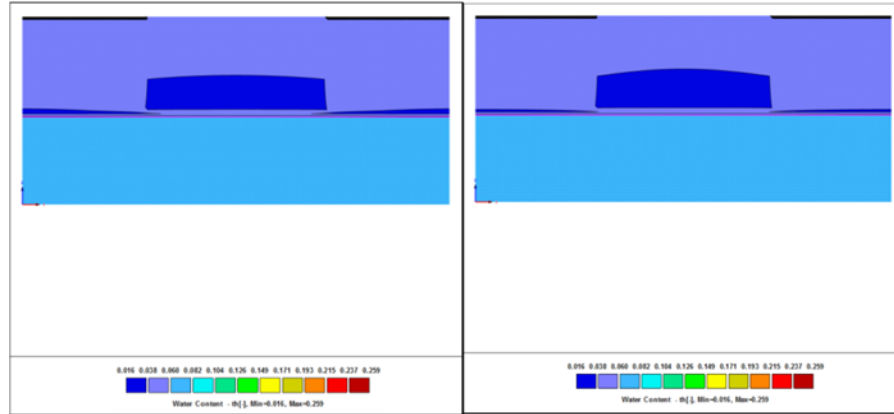
20

Figure 4-10: Simulated water content distributions at the end of *stage e* (Dec. 31, 3046) for Pit 37 scenarios 1 (left) and 2 (right). A constant recharge rate (or effective infiltration) of 0.1 mm/year is added on the top of the model.
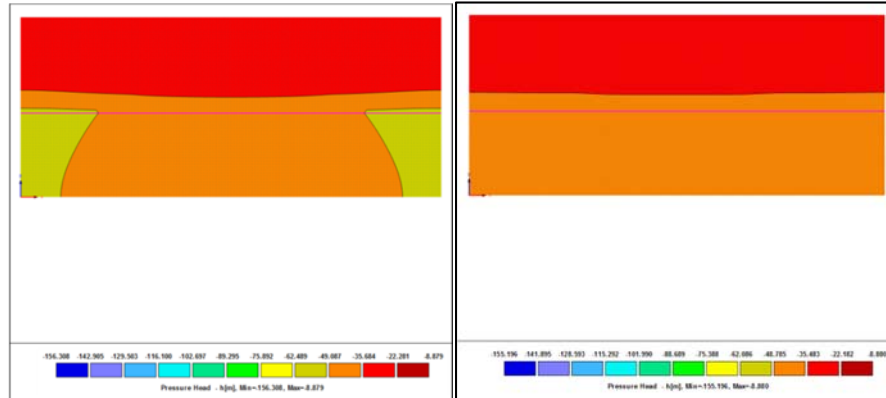

Figure 4-11: Simulated pressure head (m) distributions at the end of *stage d* (Dec. 31, 3046) for Pit 37 scenario 1 (left) and 2 (right). A constant recharge rate (or effective infiltration) of 0.1 mm/year is added on the top of the model.
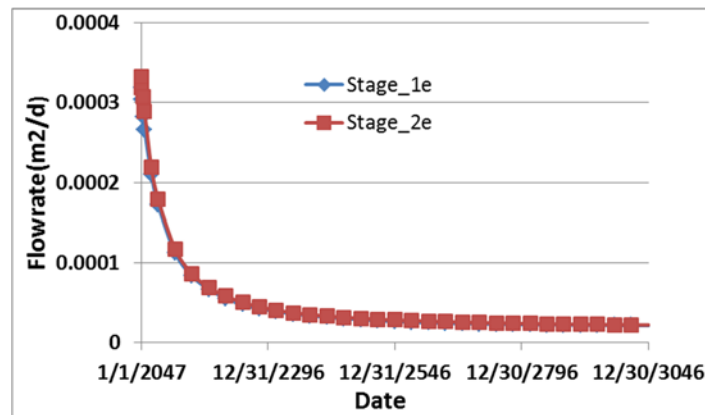

Figure 4-12: Computed water flow rates from the bottom of the Pit 37 during *stage d*.
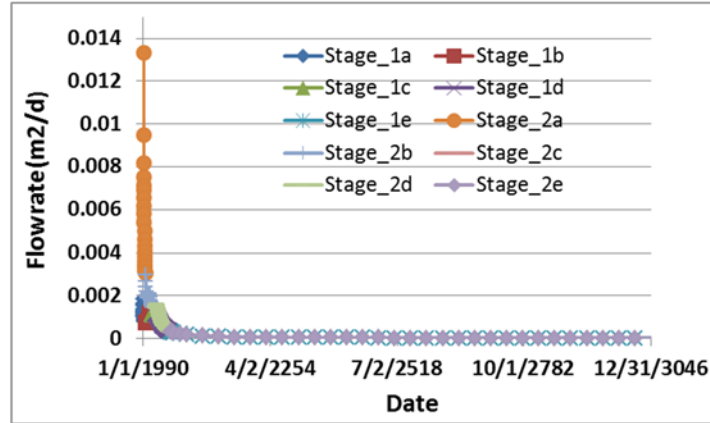
21

Figure 4-13: Computed water flow rates from the bottom of the Pit 37 for the two scenarios for all stages (*stage a* to *stage e*).
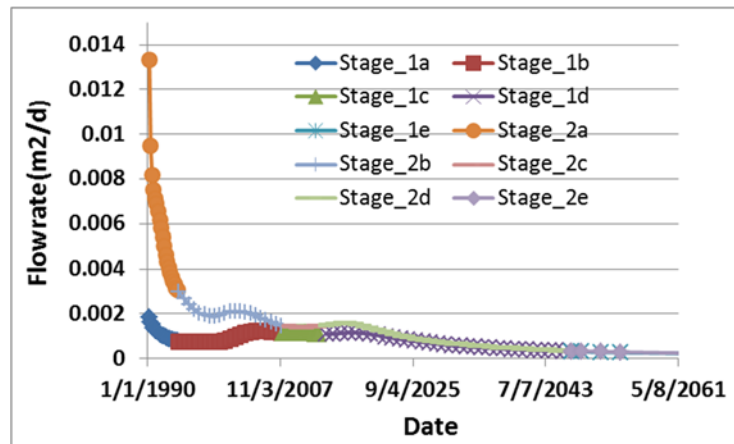

Figure 4-14: Computed water flow rates from the bottom of the Pit 37 for the two scenarios by enlarging *stage a* to early *stage e*.

4.2. Simulations for Pit 38 East

A two-dimensional cross section model is built for simulating water flow in the eastern half of Pit 38 (Pit 38 East) using three scenarios. The first two scenarios are designed to test the impact of different initial saturations (33% and 20%) on the computed flow rates across the bottom of the pit. Neutron logging data (Levitt et al., 2015) indicate that a range of 20-33% saturation is reasonable. Scenario 3 accounts for potential runoff based on field observations made on September 22, 2015, that indicated potentially significant runoff into Pit 38 East. Six stages are used for each scenario based on the progression of waste disposal in Pit 38.

Scenario 1 (Pit38E_1)

Stage a: January 1, 1994 to Dec. 31, 1999, 5-m-thick waste layer added to the bottom of Pit 38 East with initial saturation of 33%. Outside of the pit the initial hydraulic pressure of -70 m was assumed.

Stage b: January 1, 2000 to Dec. 31, 2005, 5-m-thick additional waste layer added to the pit with initial saturation of 33%.

Stage c: January 1, 2006 to December 31, 2011, 2-m-thick additional waste layer added to the pit with initial saturation of 33%.

Stage d: January 1, 2011 to December 31, 2013, 2-meter-thick additional waste layer added to the pit with initial saturation of 33%. For *Stage d,* the waste layer has modified properties assuming **a new material with high conductivity of 20 m/d and low porosity 0.01**. These properties are assumed because the waste emplaced was noted to be containerized (large metal boxes or large disposal bags) and closely spaced, and was not covered with fill during this time period. We assumed that water would flow relatively quickly through the space around the containers, and these material properties produce that effect in the HYDRUS model. Photos taken on September 19, 2013 show that the waste is uncovered. We note that the large multi-day rainfall event in September 2013 occurs during this phase.

Stage e: January 1, 2014 to Dec. 31, 2046, 2-m-thick additional waste layer added to the pit with initial saturation of 33%. The observed precipitation data from January 1, 2014 to June 30, 2015 were input to the model. From July 2015 to the end of 2046, we used the predicted daily precipitation and evaporation/transpiration (PE and PT) documented in Appendix A to cover this period for the rest of simulation of this stage. This time period represents the interim cover. We note that the interim cover was not all the way to grade in September 2015, but assume it is for this stage of the model.

Stage f: January 1, 2047 to Dec. 31, 3046, one-thousand-year prediction was conducted with a constant effective infiltration rate of 0.1 mm/year on the top of the model.

Scenario 2 (Pit38E_2)

Stage a: January 1, 1994 to Dec. 31, 1999, 5-m-thick waste layer added to the bottom of Pit 38 with initial saturation of 20%. Outside of the pit the initial hydraulic pressure of -70 m was assumed.

Stage b: January 1, 2000 to Dec. 31, 2005, 5-m-thick additional waste layer added to the pit with initial saturation of 20%.

Stage c: January 1, 2006 to December 31, 2011, 2-m-thick additional waste layer added to the pit with initial saturation of 20%.

Stage d: January 1, 2011 to December 31, 2013, 2-meter-thick additional waste layer added to the pit with initial saturation of 20%. For *Stage d,* the waste layer has modified properties assuming **a new material with high conductivity of 20 m/d and low porosity 0.01**. [See *Stage d* of scenario 1, above, for more detail about this assumption.]

Stage e: January 1, 2014 to Dec. 31, 2046, 2-m-thick additional waste layer added to the pit with initial saturation of 20%. The observed precipitation data from January 1, 2014 to June 30, 2015 were input to the model. From July 2015 to the end of 2046, we used the predicted daily precipitation and evaporation/transpiration (PE and PT) documented in Appendix A to cover this period for the rest of simulation of this stage. This time period represents the interim cover. We note that the interim cover was not all the way to grade in September 2015, but assume it is for this stage of the model.

Stage f: January 1, 2047 to Dec. 31, 3046, one-thousand-year prediction was conducted with a constant effective infiltration rate of 0.1 mm/year on the top of the model.

Scenario 3 (Pit38E_3)

Stages a to d are the same as those in Scenario 1.

Stage e: January 1, 2014 to Dec. 31, 2046, 2-meter-thick additional waste layer added to the pit with initial saturation of 33%. The observed precipitation data from January 1, 2014 to June 30, 2015 were input to the model. From July 2015 to the end of 2046, we used the predicted daily precipitation and evaporation/transpiration (PE and PT) documented in Appendix A to cover this

period for the rest of simulation of this stage. This time period represents the interim cover. We saw that the interim cover in September 2015 was not really all the way to grade. *This scenario makes an assumption to include increased run-off into the pit for a 3-year period for which we assume there is greater water coming into the pit: (1) from 1/1/2014 to 12/31/2016, assume double the precipitation rates. The pit is filled to grade in the model, but the additional precipitation accounts for a period when runoff into the pit could be significant because the pit was not actually filled to grade;* (2) from 1/1/2017 to 1/1/2047, this scenario matches Scenario 1 with the same precipitation data.

Stage f: January 1, 2047 to Dec. 31, 3046, one-thousand-year prediction was conducted with a constant effective infiltration rate of 0.1 mm/year on the top of the model.

4.2.1 *Stage a* **simulations – Pit 38 East**

A two-dimensional model is built for the Pit 38 East *stage a* simulations (see Figure 4-15). After running the model from January 1, 1994 to Dec. 31, 1999, we compare the modeling results for the first two scenarios. Figure 4-16 shows the final simulated pressure head (m) distributions at the end of *stage a* (Dec. 31, 1999) for the two Pit 38 East scenarios. With larger initial saturation for the waste in scenario 1, the water infiltrates deeper than for scenario 2, and the flow rate across the bottom of Pit 38 East for scenario 1 is much larger than for scenario 2. Figure 4-17 is the computed water flow rates across the pit bottom from the two scenarios. The flow rates across the bottom of the pit are similarly different because the initial saturations of the waste layer are different in the two scenarios. However, both scenarios have the same recharge conditions (same precipitation rate). At the end of *stage a*, the flow rates across the bottom of the pit are similar for the two scenarios.
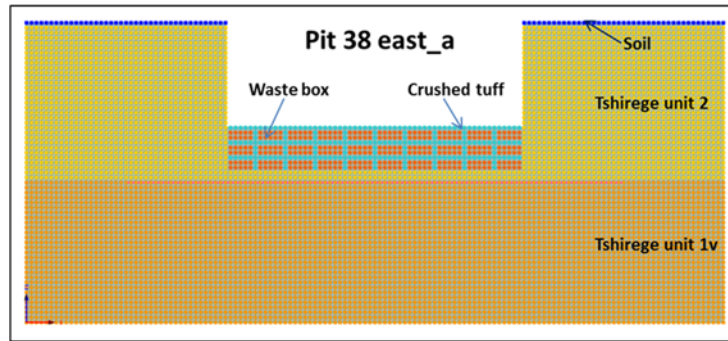
Figure 4-15: A two-dimensional numerical model for simulating water flow in Pit 38 East. The model has a size of 70x30m². The pit size is 15 m deep, 30 m wide on the top. The light blue and red-box area in the pit represents the filled waste (5 m thick) in *stage a*, with initial saturations of 33% and 20% for scenarios 1 and 2, respectively. The red line (right below the pit bottom) is an auxiliary mesh line for computing the flow rates across the pit bottom.
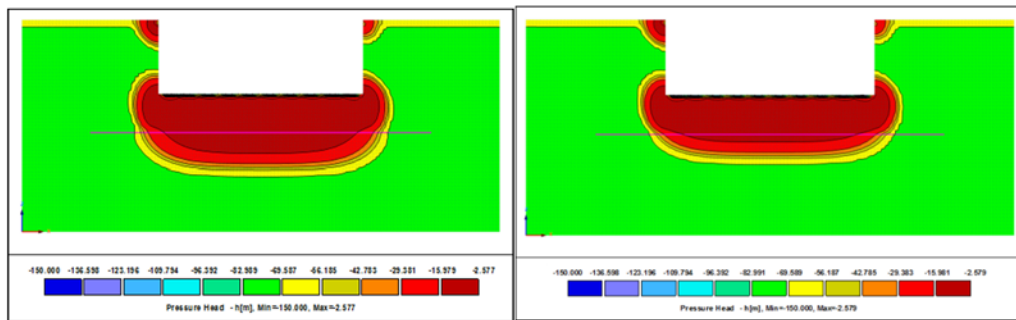

Figure 4-16: Simulated pressure head (m) distributions at the end of *stage a* (Dec. 31, 1999) for Pit 38 East scenarios 1 (left) and 2 (right)
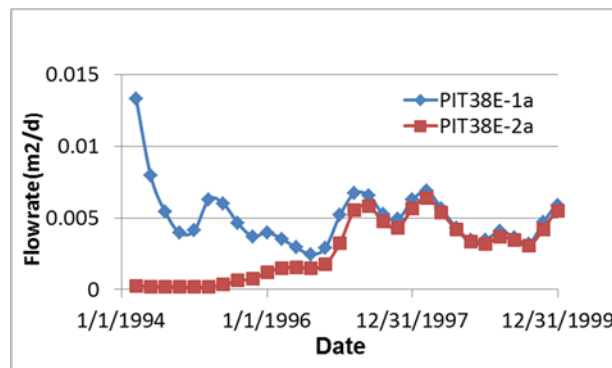

Figure 4-17: Computed water flow rates from the bottom of the Pit 38 East during *stage a* for scenarios 1 (blue) and 2 (red)

26

4.2.2 *Stage b* simulations – Pit 38 East

In *stage b,* we add a 5-m-thick additional waste into Pit 38 East. The initial condition was input from the result of *stage a* (Dec. 31, 1999, of the two scenarios), while the newly added waste has an initial saturation of 33% and 20% for two scenarios, respectively. The simulated pressure head distributions at the end of *stage b* (Dec. 31, 2005) are shown in Figure 4-18. The computed water flow rates from the pit bottom are plotted in Figure 4-19. Scenario 1, with much larger initial saturation for the waste layer, has much more water flow across the bottom of Pit 38 East in early time, but the flow rates computed from the two scenarios become more similar with time.
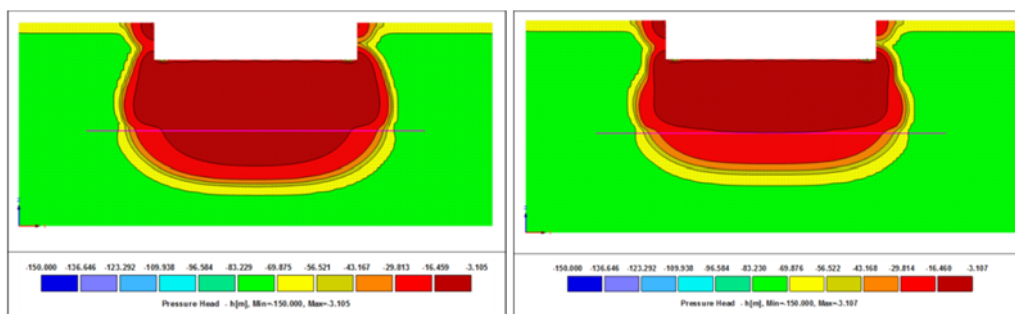

Figure 4-18: Simulated pressure head (m) distributions at the end of *stage b* (Dec. 31, 2005) for Pit 38 East scenarios 1 (left) and 2 (right).
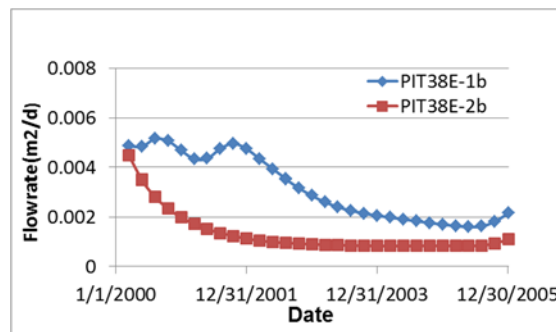

Figure 4-19: Computed flow rates from the bottom of the Pit38 East during *stage b* for Scenarios 1 (blue) and 2 (red).

4.2.3 *Stage c* simulations – Pit 38 East

In *stage c,* we add an additional 2-m-thick waste layer onto the other waste layers in Pit 38 East. The initial condition was input from the results of *stage b*, while the newly added waste has an initial saturation of 33% and 20% for the two scenarios, respectively. The simulated pressure

27

head distributions at the end of *stage c* (Dec. 31, 2010) are shown in Figure 4-20. The computed water flow rates from the pit bottom are plotted in Figure 4-21.
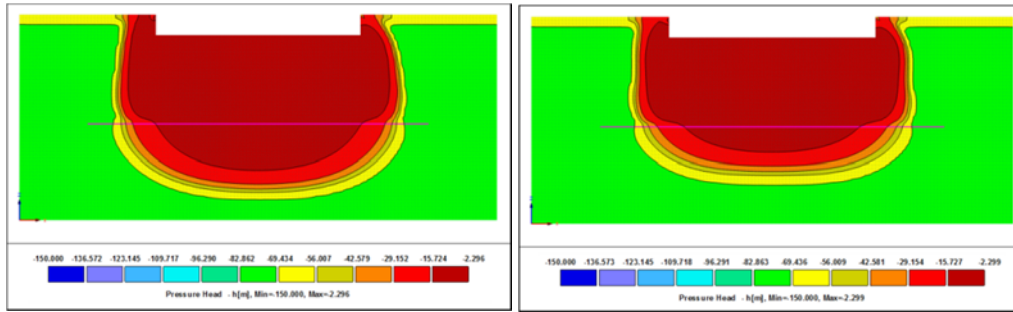

Figure 4-20: Simulated pressure head (m) distributions at the end of *stage c* (Dec. 31, 2010) for Pit 38 East and for both scenarios 1 (left) and 2 (right).
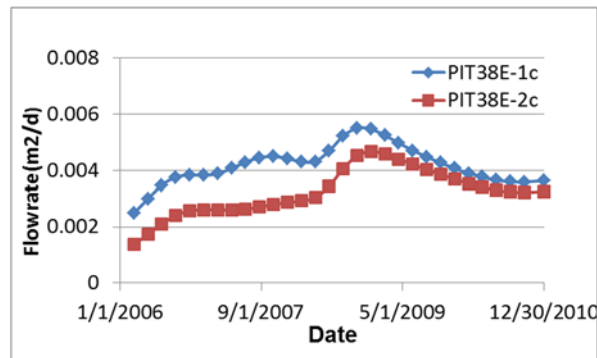

Figure 4-21: Computed water flow rates from the bottom of the Pit 38 East during *stage c* for scenarios 1 (blue) and 2 (red).

4.2.3 *Stage d* simulations – Pit 38 East

In *stage d,* we add an additional 2-m-thick waste layer with initial saturation of 33% and 20% for the two scenarios, respectively. The end results (pressure distributions) from *stage c* are used as the initial conditions to run the model until December 31, 2013. In *Stage d,* the waste is treated as a new material with high conductivity (20 m/d) and low porosity (0.01) so that water percolates quickly through this layer. The simulation includes the impact of the large rainfall event in September 2013 on the flow rates across the bottom of the pit. The simulated pressure head distributions at the end of *stage d* (Dec. 31, 2013) are shown in Figure 4-22 for the two scenarios, respectively. The computed water flow rates from the pit bottom are plotted in Figure 4-23, which shows that after 5 years, the flow rates across the bottom of Pit 38 East for both scenarios are similar. The difference of the initial saturation has an impact to the flow rates for

28

the first three years in this stage and then precipitation and infiltration conditions dominate the flow rates.
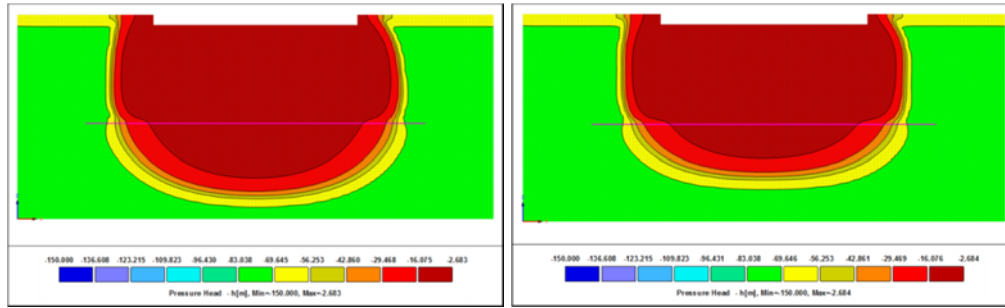

Figure 4-22: Simulated pressure head (m) distributions at the end of *stage d* (Dec. 31, 2013) for scenarios 1 (left) and 2 (right).
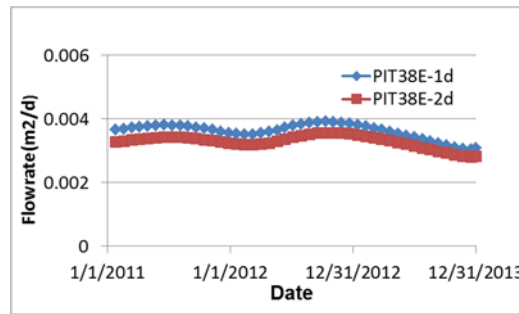

Figure 4-23: Computed water flow rates from the bottom of the Pit 38 East during *stage d* for both scenarios.

4.2.4 *Stage e* simulations – Pit 38 East

In *stage e,* we add an additional two-m-thick waste layer in the pit with initial saturation of 33% and 20% for scenarios 1 and 2, respectively. This stage represents the interim cover time period from 1/1/2014 to 1/1/2047 for 33 years. The interim cover in September 2015 was observed to be lower than grade (ground level). To consider this condition, we assume a new precipitation scheme (scenario 3 with the same initial conditions as scenario 1) to represent increased runoff into the pit for a 3-year period (1/1/2014 to 12/31/2016) over which we assume there is greater water (two times larger precipitation rates than used in scenarios 1 and 2, based on our observations on 9/22/2015 that significant runoff into Pit 38 East may have been occurring) coming into the pit, while from 1/1/2017 to 1/1/2047, scenario 3 matches scenario 1 with the same precipitation rate. The end results (pressure distributions) of *stage d* for the three scenarios are used as the initial conditions, respectively, to run the three scenarios until December 31, 2047.

The simulated pressure head distributions at the end of *stage e* (Dec. 31, 2047) are shown in Figure 4-24 for the three scenarios, respectively. The computed water flow rates from the pit bottom are plotted in Figure 4-25, which shows that for scenario 3, the computed flow rates during the 1/1/2014 to 12/31/2016 time period are much larger than those for the first two scenarios. After 20 years, the flow rates across the bottom of Pit 38 East for the three scenarios are similar.
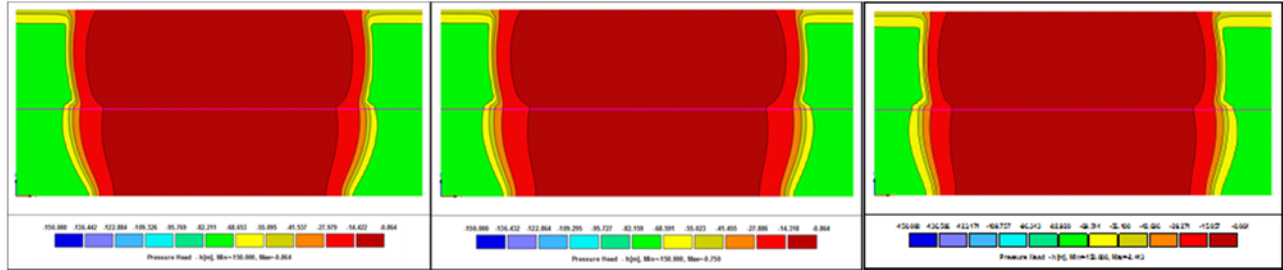

Figure 4-24: Simulated pressure head (m) distributions at the end of *stage e* (Dec. 31, 2047) for Pit 38 East scenarios 1 (left), 2 (middle), and 3 (right).
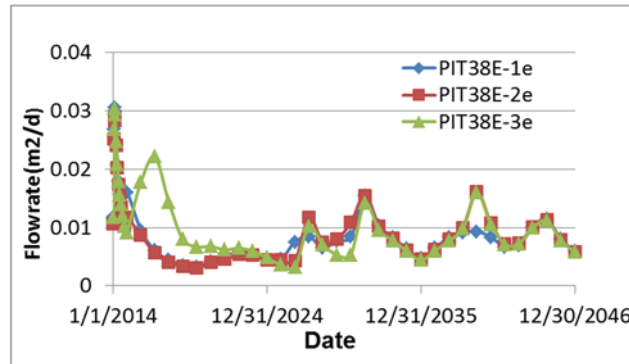

Figure 4-25: Computed water flow rates from the bottom of Pit 38 East during *stage e* for scenarios 1 (blue), 2 (red), and 3 (green).

4.2.5 Stage f simulations – Pit 38 East

In *stage f,* we use the end results (pressure distributions) of *stage e* as initial conditions to run the three scenarios for one thousand years. The effective infiltration rate of 0.1 mm/year was added to the model top as a constant flow rate boundary. The simulated pressure head distributions at the end of *stage f* (Dec. 31, 3046) are almost identical for the three scenarios (Figure 4-26). The computed water flow rates from the pit bottom are plotted in Figure 4-27. The computed flow

rates from the three scenarios are very similar in the later part of this stage. The combined water flow rates from the pit bottom during all stages (*stages a to f*) are plotted in Figures 4-28 and 4-29.
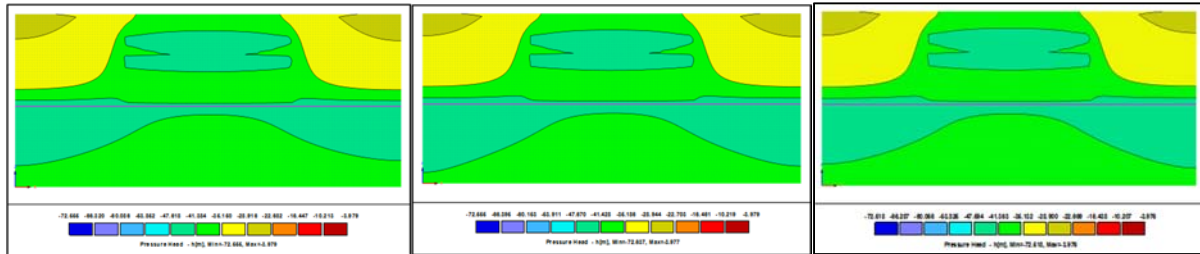

Figure 4-26: Simulated pressure head (m) distributions at the end of *stage e* (Dec. 31, 3046) for Pit 38 East scenarios 1 (left), 2 (middle), and 3 (right).
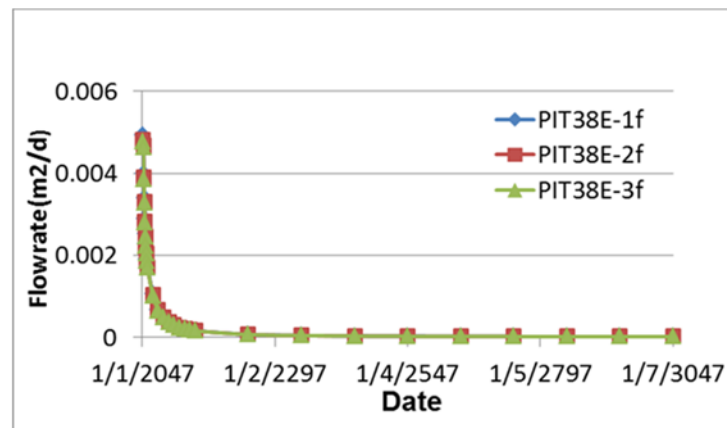

Figure 4-27: Computed water flow rates from the bottom of Pit 38 East during *stage e* for scenarios 1 (blue), 2 (red), and 3 (green).
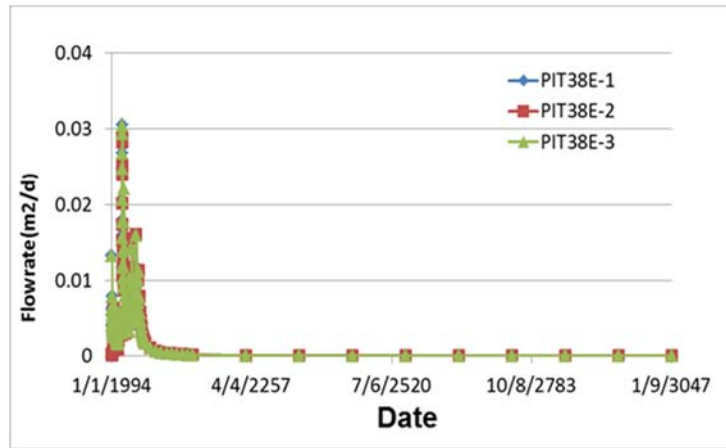
Figure 4-28: Computed water flow rates from the bottom of Pit 38 East for the entire modeling period (*stages a* to *f*) for scenarios 1 (blue), 2 (red), and 3 (green).
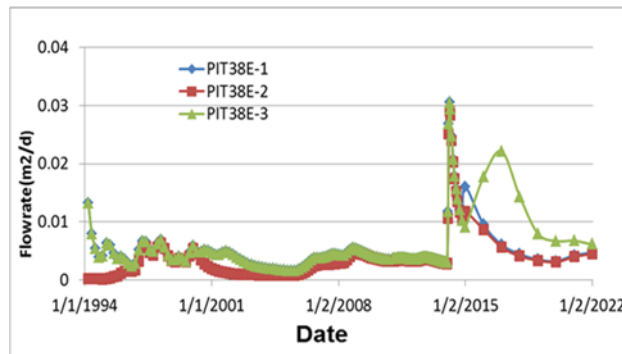

Figure 4-29: Computed water flow rates from the bottom of the Pit 38 East for scenarios 1 (blue), 2 (red), and 3 (green), enlarging *stage a* to early *stage e*.

4.3   Simulations for Pit 38 West

A two-dimensional, cross-sectional model is built for simulating water flow through Pit 38 West (Pit 38w) with HYDRUS (v2.03, Simunek and Sejna, 2011). Six stages are modeled based on the progression of waste disposal in Pit 38 and the closure plan for an interim cover. Only one scenario, with higher initial waste saturation of 33%, is run for Pit 38 West.

Stage a: January 1, 1994 to Dec. 31, 1999, 5-m-thick waste layer added to the bottom of Pit 38 West with initial saturation of 33%. Outside of the pit the initial hydraulic pressure of -70 m was assumed.

Stage b: January 1, 2000 to Dec. 31, 2005, 5-m-thick additional waste layer added to the pit with initial saturation of 33%.

Stage c: January 1, 2006 to December 31, 2011, 2-m-thick additional waste layer added to the pit with initial saturation of 33%.

Stage d: January 1, 2011 to December 31, 2013, 2-m-thick additional waste layer added to the pit with initial saturation of 33%. Contaminant control water (dust suppression plus decontamination water; 1649 m^3 during June 2011 to February 2012) was input to the top of the waste in this stage. We assigned the contaminant control water to the top of the waste on one day (September 21, 2011) as a precipitation event.

Stage e: January 1, 2014 to Dec. 31, 2046, 2-meter-thick additional waste layer added to the pit with initial saturation of 33%. The observed precipitation data from January 1, 2014 to June 30, 2015 were input to the model. From July 2015 to end of 2046, we used the predicted daily precipitation and evaporation/transpiration (PE and PT) (Appendix A) for the simulation of this portion of the stage. Note that this time period represents the interim cover.

Stage f: January 1, 2047 to Dec. 31, 3046, one-thousand-year prediction was conducted with a constant effective infiltration rate of 0.1 mm/year on the top of the model.

4.3.1 Stage a simulations – Pit 38 West

A two-dimensional model is built for *stage a* simulations (see Figure 4-30). After running the model from January 1, 1994 to Dec. 31, 1999, we plot the final simulated pressure head (m) distributions at the end of *stage a* (Figure 4-31). Figure 4-32 is the computed water flow rates across the pit bottom for the two scenarios. Since the initial saturation of the waste is high (33%), the flow rates across the bottom of the pit are high in the initial time and then vary with the precipitation rates.
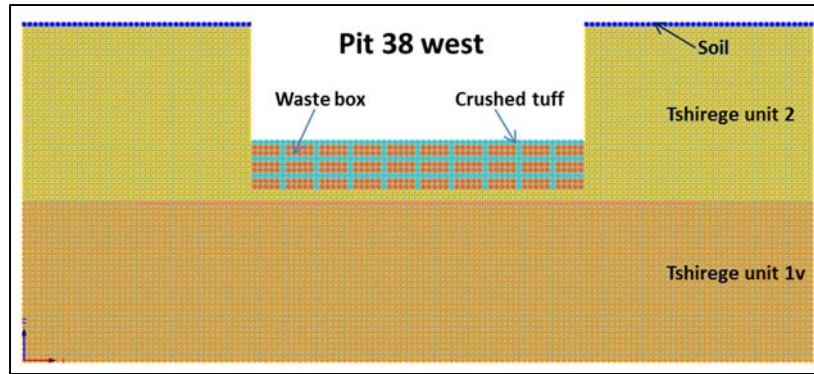
Figure 4-30: A two-dimensional numerical model for simulating water flow in Pit 38 West. The model has a size of 70x30m². The pit size is 15 m deep, 30 m wide on the top. The light blue and red-box area in the pit represents the filled waste (5 m thick) in *stage a*, with initial saturations of 33%. The red line (right below the pit bottom) is an auxiliary mesh line for computing the flow rates from the bottom of the waste pit.
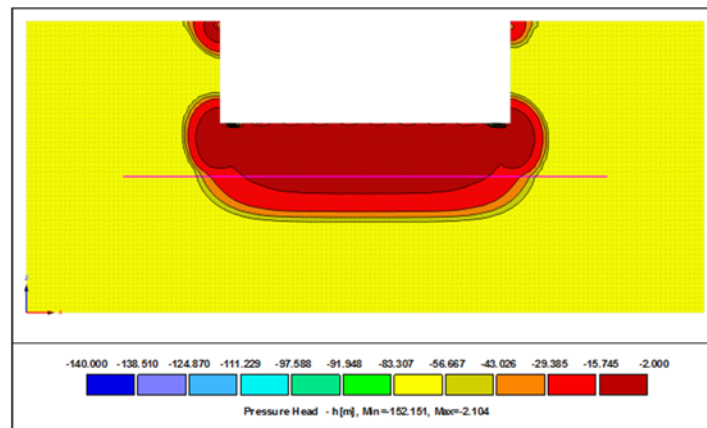

Figure 4-31: Simulated pressure head (m) distributions at the end of *stage a* (Dec. 31, 1999)
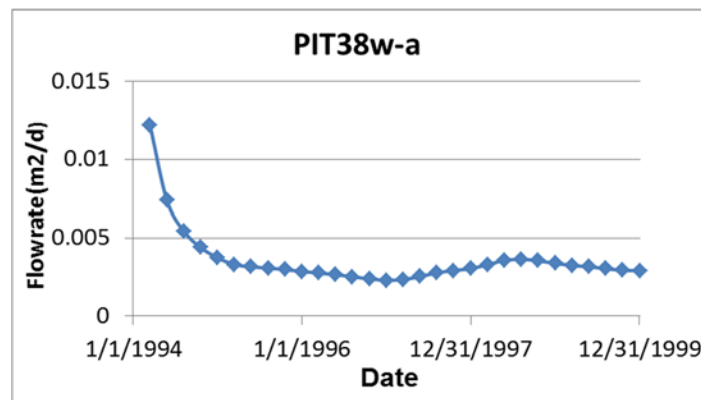

Figure 4-32: Computed water flow rates from the bottom of the Pit 38 West during *stage a*.

4.3.2 *Stage b* simulations – Pit 38 West

In *stage b,* we add a 5-meter-thick waste layer into the pit. The initial condition was input from the end result of *stage a* (Dec. 31, 1999), while the newly added waste has an initial saturation of 33%. The simulated pressure head distribution at the end of *stage b* (Dec. 31, 2005) is shown in Figure 4-33. The computed water flow rates from the pit bottom are plotted in Figure 4-34. The water flow rates across the bottom of the Pit 38 West are high in the early time due to the relatively larger initial saturation for the newly filled waste, and then reduce gradually with time.
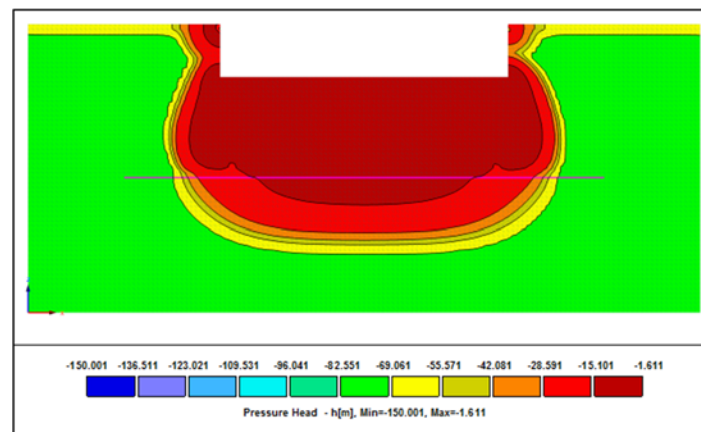

Figure 4-33: Simulated pressure head (m) distributions at the end of *stage b* (Dec. 31, 2005)

Figure 4-34: Computed flow rates from the bottom of the Pit 38 West during *stage b*.

4.3.3 *Stage c* simulations – Pit 38 West

In *stage c,* we add a 2-meter-thick waste layer added to the pit. The initial condition was input from the end result of *stage b*, while the newly added waste has an initial saturation of 33%. The simulated pressure head distribution at the end of *stage c* (Dec. 31, 2010) is shown in Figure 4-35. The computed water flow rates from the pit bottom are plotted in Figure 4-36.

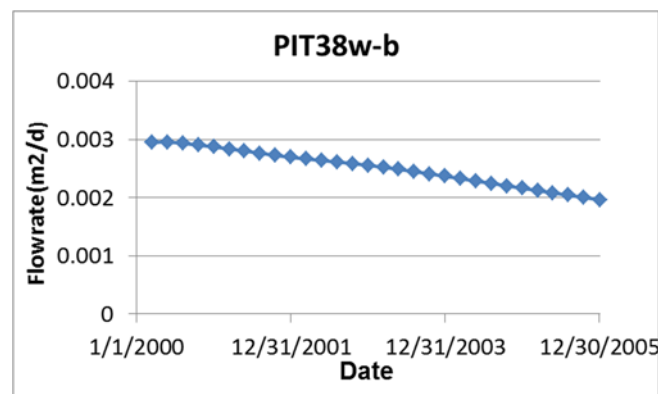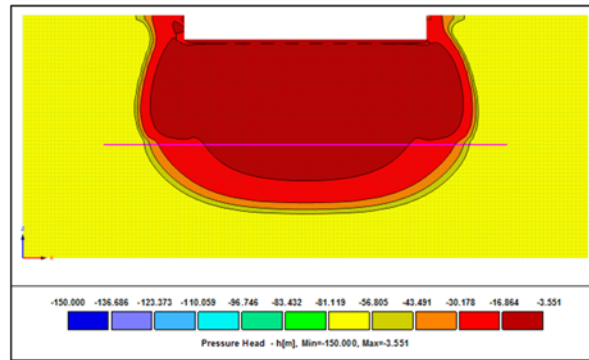Figure 4-35: Simulated pressure head (m) distributions at the end of *stage c* (Dec. 31, 2010).
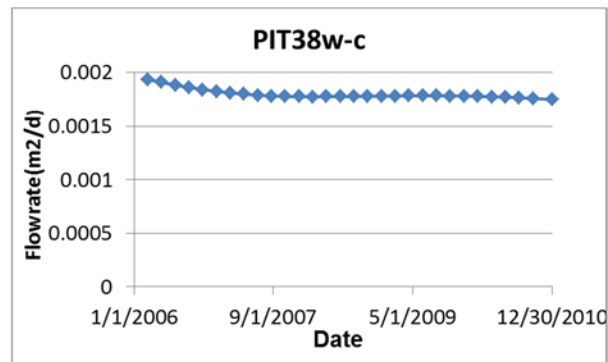

Figure 4-36: Computed water flow rates from the bottom of the Pit 38 West during *stage c*.

4.3.4 *Stage d* simulations – Pit 38 West

In *stage d,* we add two meters of waste with initial saturation of 33% to the pit. The pressure distribution result of *stage c* was used as the initial condition to run the model until December 31, 2013. Contaminant control water with a volume of 1649 m^3 of (dust suppression plus decontamination water; during June 2011 to February 2012) was assigned to the top of the waste on one day (September 21, 2011) as a precipitation event. The simulated pressure head distribution at the end of *stage d* (Dec. 31, 2013) is shown in Figure 4-37. The computed water flow rates from the pit bottom are plotted in Figure 4-38, which shows that the contaminant control water (assigned on September 21, 2011) had a big impact on the flow rates across the bottom of Pit 38 West, and the flow rates increase three months after input of the contaminant control water.
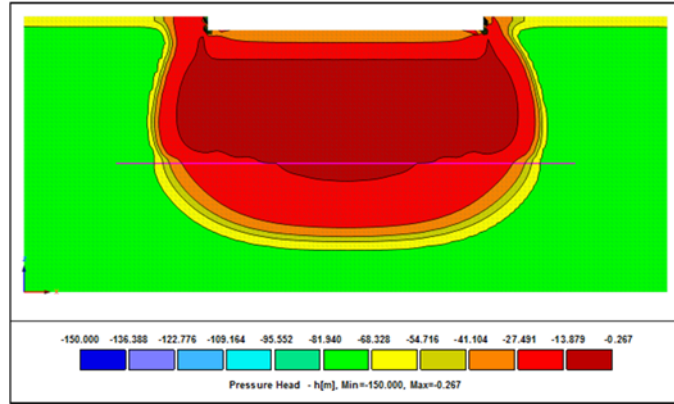
36

Figure 4-37: Simulated pressure head (m) distributions in Pit 38 West at the end of *stage d* (Dec. 31, 2013).
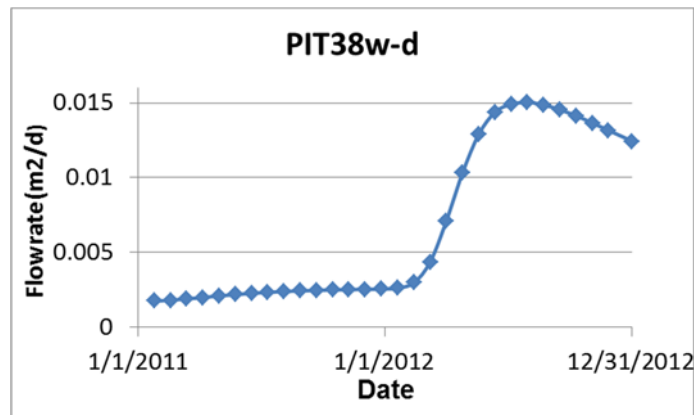

Figure 4-38: Computed water flow rates from the bottom of the Pit 38 West during *stage d*.

4.3.5 *Stage e* simulations – Pit 38 West

In *stage e,* we add two meters of additional waste with initial saturation of 33% to the pit. This stage represents the interim cover time period from 1/1/2014 to 1/1/2047 for 33 years. The end pressure distribution result for *stage d* was used as the initial condition to run the model until December 31 of 2047. The observed precipitation rates from 1/1/2014 to 6/30/2015 and the predicted daily precipitation and evaporation/transpiration (PE and PT) (Appendix A) from July 2015 to the end of 2046 were used to cover this period. The simulated pressure head distribution at the end of *stage e* (Dec. 31, 2047) is shown in Figure 4-39. The computed water flow rates from the pit bottom are plotted in Figure 4-40, which shows that the flow rates across the bottom of Pit 38 West are mainly influenced by the precipitation rates.

37

Figure 4-39: Simulated pressure head (m) distributions for Pit 38 West at the end of *stage e* (Dec. 31, 2047).
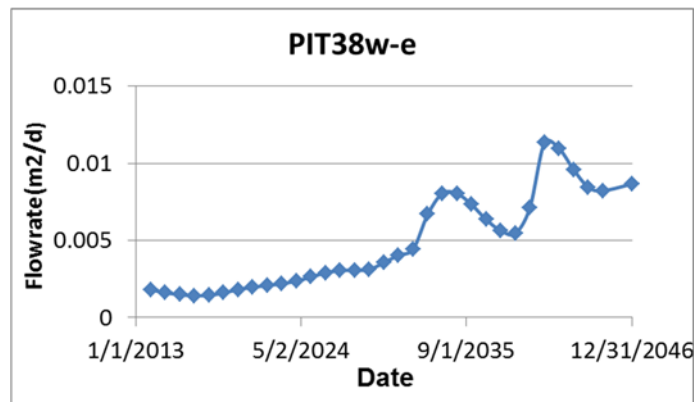
Figure 4-40: Computed water flow rates from the bottom of Pit 38 West during *stage e*.

4.3.6 *Stage f* simulations – Pit 38 West

In *stage f,* we use the end pressure distribution result of stage e as the initial condition to run the model for one thousand years. The effective infiltration rate of 0.1 mm/year was added to the model top as a constant flow rate boundary. The simulated pressure head distribution at the end of *stage f* (Dec. 31, 3046) is plotted in Figure 4-41. The computed water flow rates from the pit bottom are plotted in Figure 4-42. The combined water flow rates from the pit bottom during the entire modeling time (*stages a to f*) are plotted in Figures 4-43 and 4-44.
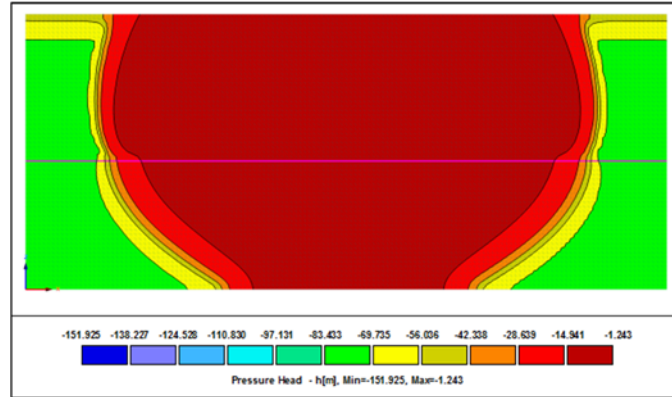
Figure 4-41: Simulated pressure head (m) distributions for Pit 38 West at the end of *stage f* (Dec. 31, 3046).

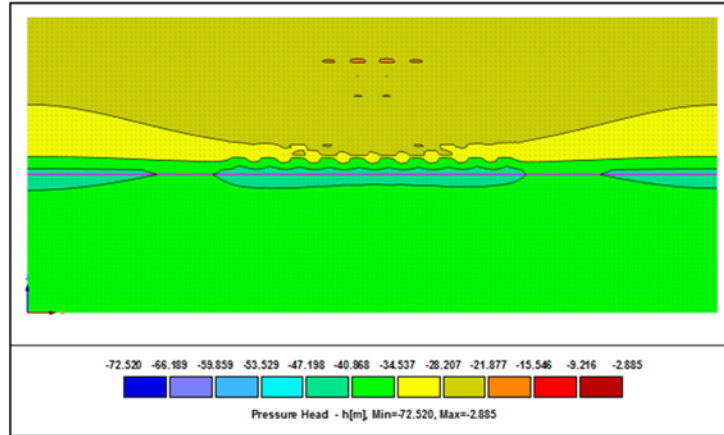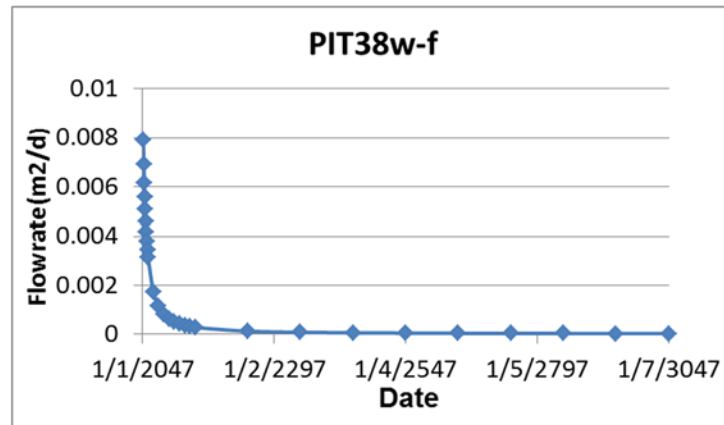Figure 4-42: Computed water flow rates from the bottom of Pit 38 West during *stage f*.
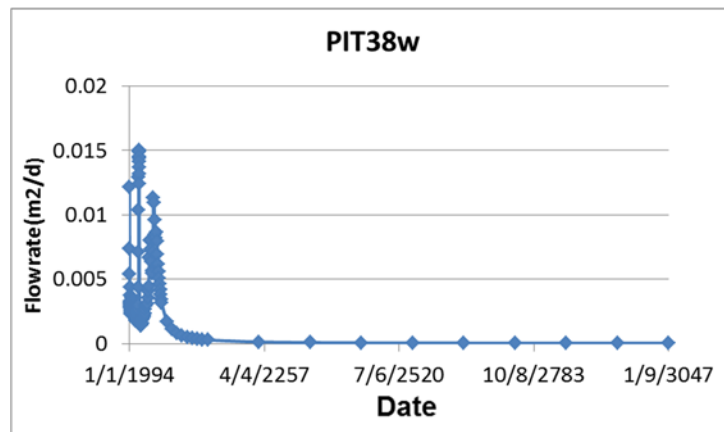

Figure 4-43: Computed water flow rates from the bottom of Pit 38 West for all modeling stages (*stages a to f*).
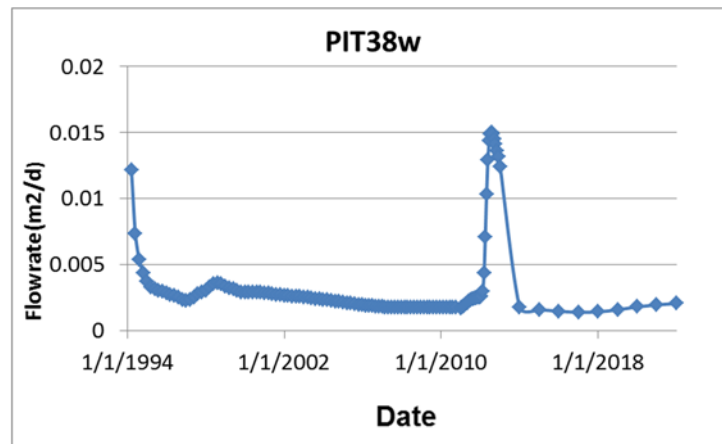
Figure 4-44: Computed water flow rates from the bottom of Pit 38 West by enlarging *stage a* to early *stage e*.

4.3   Simulations for the Pit 38 Extension

A two-dimensional, cross-sectional model is built for simulating water flow through the bottom of the Pit 38 extension (Pit38x) with HYDRUS (v2.03, Simunek and Sejna, 2011). One scenario is modeled that includes four stages based on expected waste disposal and placement of an interim cover:

Stage a: July 1, 2012 to May 11, 2014. The pit was dig to 11-m deep, 20-m wide on the top and 18-m wide at the bottom. No waste was disposed during this time period (i.e., the pit was open). A precipitation or atmosphere boundary condition is used for the top of the model during this stage. The bottom of the domain has a free drainage boundary. The left and right sides of the domain use no-flow boundary conditions. We first run the model with a constant infiltration rate of 0.1 mm/year on the top of the model to reach a steady state, which is used as the initial condition for *stage a*. The comparison of the simulated and observed hydraulic pressures was presented in section 3.

Stage b: May 12, 2014 to December 31, 2016. An approximate 8-meter-thick waste layer was added to the bottom of the pit with initial saturation of 10%. The waste was assumed to be added all at once on May 12, 2014. A drier saturation is used than for Pits 37, 38 East and 38 West because of recommendations made to operators from the PA modeling team. Contaminant control water (78 m^3 or 20649 gallon) was input to the top of the waste in a single day (June 15,

2014) as a precipitation event. This volume of water represents a practical, yet minimum, amount assumed for dust suppression. Actual precipitation was used from May 12, 2014 through June 30, 2015. The predicted precipitation and evaporation/transpiration (PE and PT) was used from July 1, 2015 to December 31, 2016 (Appendix A). We added three observation points (1.05 m, 1.65 m, and 2.15 m beneath the bottom of the pit) for comparing the computed hydraulic pressure with the corresponding measurements (Results were shown in section 3).

Stage c: January 1, 2017 to December 31, 2046. An approximate 3-meter-thick crushed tuff cover is assumed to be added to the pit on January 1, 2017 with initial saturation of 33%. Pit38x is assumed to be fully covered at that time. The predicted precipitation and evaporation/transpiration (PE and PT, See Appendix A) were used to simulate the entire period. Plant water uptake is assigned to the two sides of the pit; we assume no plants on the top of the pit during this time period.

Stage d: January 1, 2047 to December 31, 3046, One-thousand-year prediction was conducted with a constant effective infiltration rate of 0.1 mm/year to represent a final ET cover.

During these four stages, we output the water flow rates from the bottom of Pit38x, which will is used as input for the 3-dimensional FEHM simulations in this area (Pawar et al., 2018).

4.3.1 *Stage a* and model validation – Pit 38 Extension

By using the geological framework model and the corresponding parameters obtained by Levitt (2011; 2013), we built a 2-D model for *stage a* simulations (see Figure 4-45). We first ran the model with a constant infiltration rate of 0.1 mm/year on the top to reach a steady-state pressure distribution, which is used as the initial condition of this stage (Figure 4-46). The precipitation data from July 1, 2012 to February 24, 2015 are shown in Figure 3-11. During that time period, hydraulic pressure measurements are used for model validation (see section 3).

After running the model from July 1, 2012 to May 11, 2014, we can see that our model mimics the major trends of the variations in matric potential at different depths, especially for the large rainfall event that occurred in September of 2013 (Figure 3-12). The potential increase after the rainfall is clear, and our model is more sensitive to the storm than the observation data indicate. Figure 4-47 shows the final simulated pressure head (m) distributions at the end of *stage a* (May

11, 2014). Figure 4-48 shows the computed water flow rates from the pit bottom. The impact of the 2013 rainfall is incorporated in the computed flow rates.

Pit38x_a
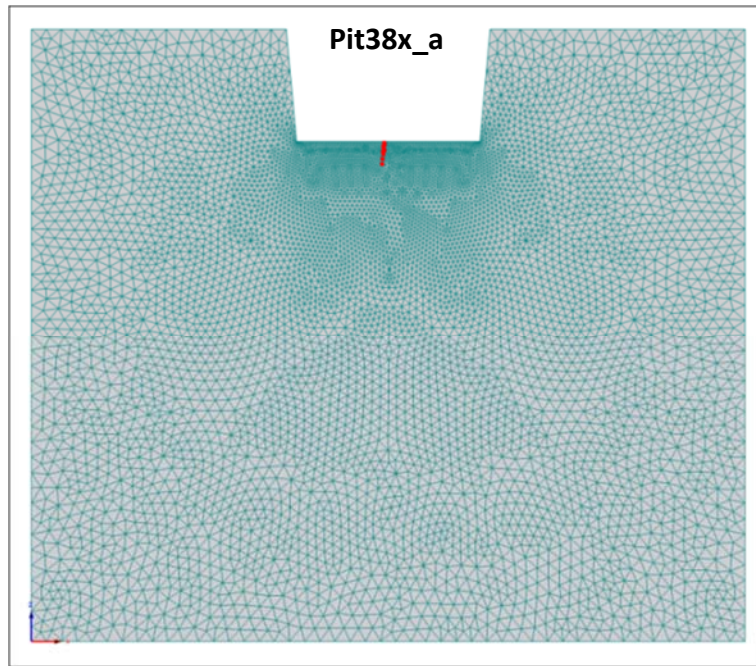
Figure 4-45: A two-dimensional numerical model for simulating water flow in the Pit 38 extension. The model has a size of 70 x 60 m^2. The pit size is 11 m deep, 20 m wide on the top and 18 m at the bottom.
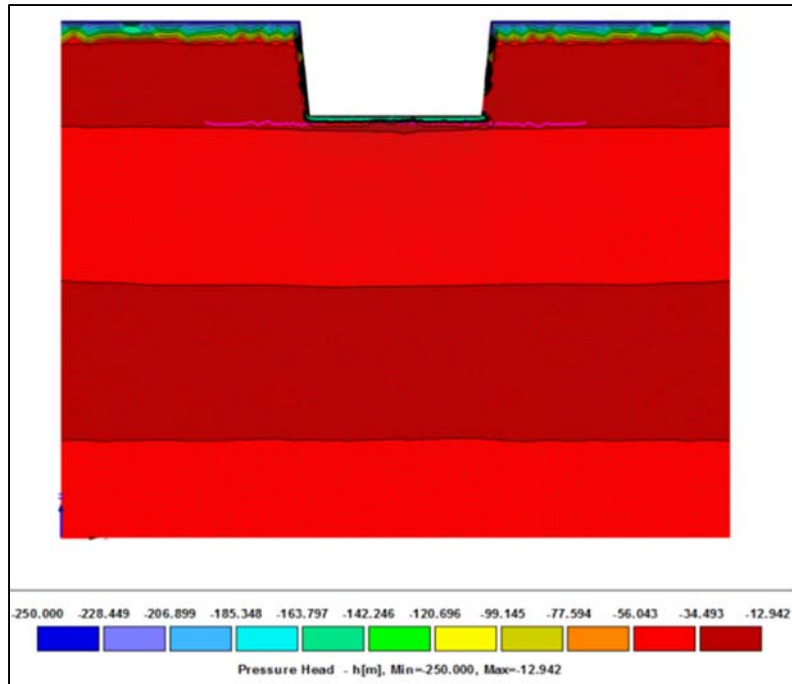
Figure 4-46: The initial hydraulic pressure distribution obtained by running the model with a constant infiltration rate of 0.1 mm/year to reach a steady state

Figure 4-47: Simulated pressure head (m) distributions for the Pit 38 extension at the end of *stage a* (May 11, 2014)

Figure 4-48: Computed water flow rates from the bottom of the Pit 38 extension during *stage a*.

4.3.2 *Stage b* simulations – Pit 38 Extension

For modeling of *stage b*, we add an 8-m-thick layer of waste into the pit on the first day of the stage (May 12, 2014). The initial condition for most of the domain was input from the end results of 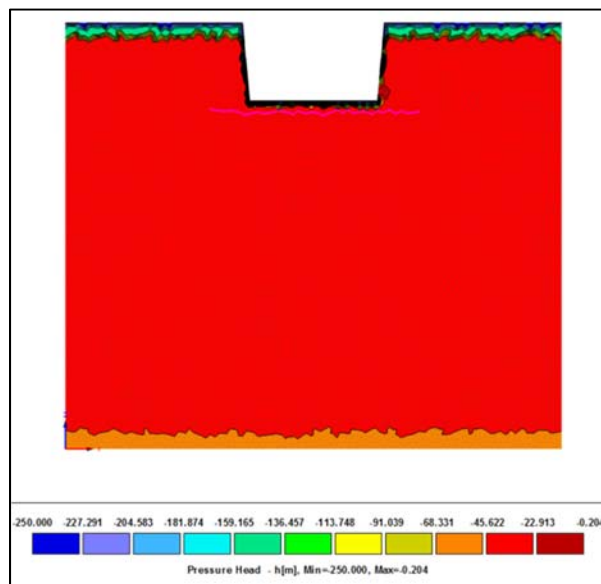*stage a*, while the newly added waste has an initial saturation of 10% (Figure 4-49). The predicted precipitation and evaporation/transpiration (PE and PT) was used from July 1, 2015 to December 31, 2016 (Appendix A). The simulated pressure head distributions at the end of *stage b* (Dec. 31, 2016) are shown in Figure 4-50. The simulated pressures at the three observation points (1.05, 1.65, and 2.15 m beneath the bottom of the pit, respectively) are output for comparing with the corresponding measurements (Figure 3-12). During this stage, the contaminant control water of 78 m^3 (20649 gallon) was added to the top of the waste on June 15, 2014. The computed water flow rates from the pit bottom are plotted in Figure 4-51.

44

Figure 4-49: The initial pressure head distributions for Pit 38 extension *stage b* (converted from end of *stage a*, May 11, 2014). The initial saturation for the new 8-m waste layer is assumed to be 10%.
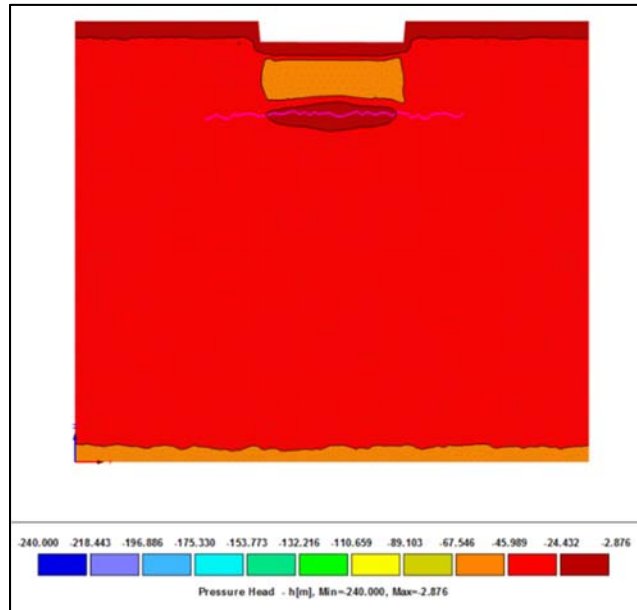
Figure 4-50: Simulated pressure head (m) distributions for Pit 38 extension at the end of *stage b* (Dec. 31, 2016). The contaminant control water of 78 m^3 (20649 gallon) was add to the top of the waste on June 15, 2014.
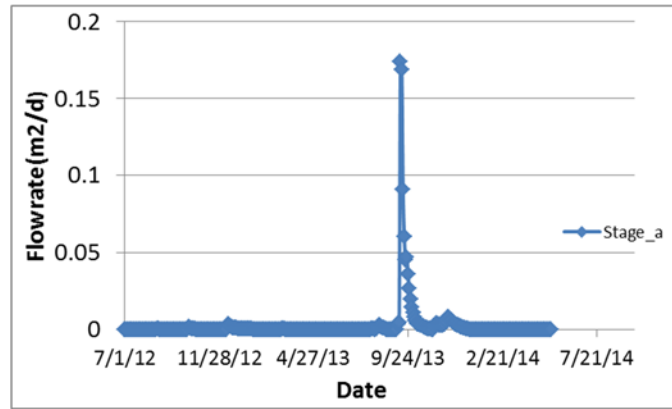
Figure 4-51: Computed water flow rates from the bottom of the Pit 38 extension during *stage b*.

4.3.1. Stage c simulations

In *stage c*, we add 3-m-thick crushed tuff cover on top of the pit. The initial condition for the rest of the domain was input from the result of *stage b*, while the newly added cover material has an initial saturation of 33% (Figure 4-52). The simulated pressure head distribution at the end of *stage c* (Dec. 31, 2046) is shown in Figure 4-53. During this stage, the predicted precipitation and evaporation/transpiration were added to the top of the model (Appendix A). The computed water flow rates from the pit bottom are plotted in Figure 4-54.
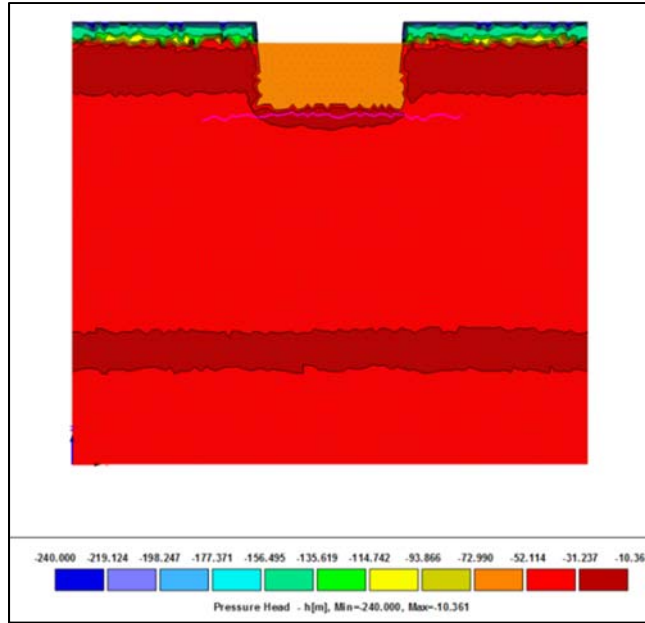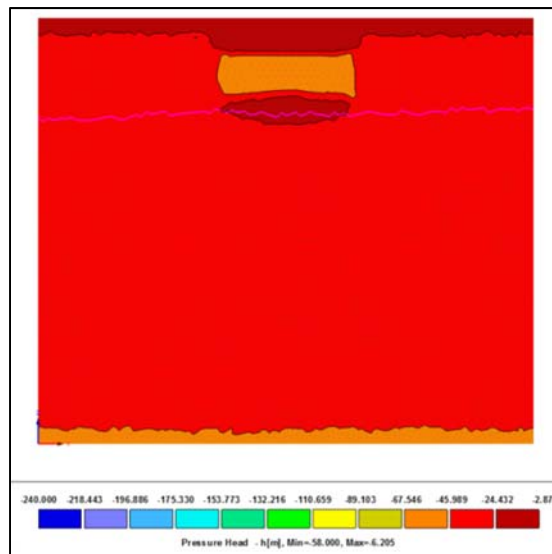

Figure 4-52: The initial water pressure (m) distributions for Pit 38 extension for *stage c* (converted from end of *stage b*, Dec. 31, 2016). The initial saturation for the cover material (3-meter thick) is assumed to be 33%.

46

Figure 4-53: Simulated pressure head (m) distribution for Pit 38 extension at the end of *stage c* (Dec. 31, 2046). Predicted daily-based precipitation and evaporation/transpiration are added on the top of the model.
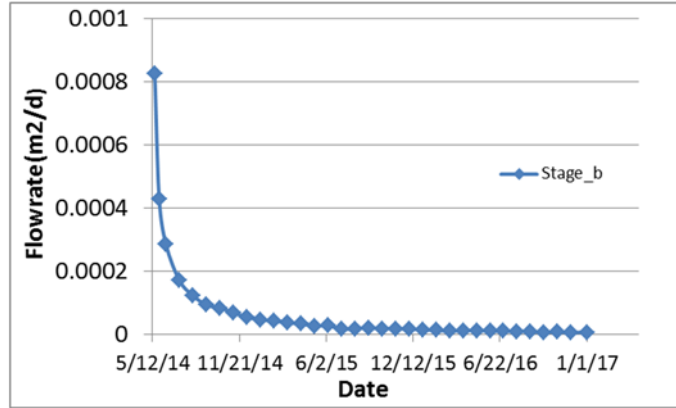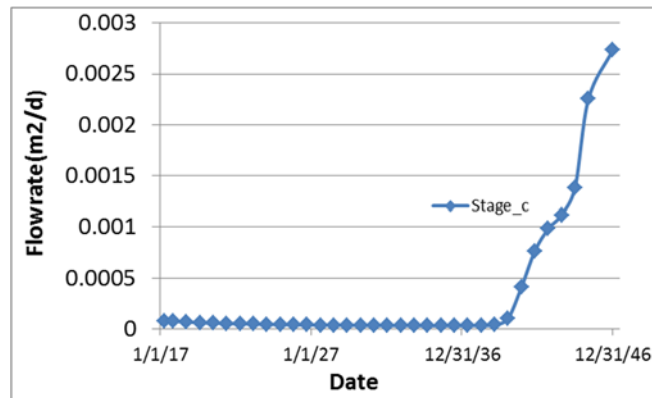

Figure 4-54: Computed water flow rates from the bottom of the Pit 38 extension during *stage c*.

4.3.3 *Stage d* simulations – Pit 38 Extension

In *stage d*, we used the pressure distributions result for *stage c* as an initial condition to run the model for one thousand years. An effective infiltration rate of 0.1 mm/year was added to the model top as a constant flow rate boundary. We also consider root uptake on the two sides of the pit. The simulated water content and pressure head distributions at the end of *stage d* (Dec. 31, 3046) are shown in Figures 4-55 and 4-56, respectively. The computed water flow rates from the pit bottom are plotted in Figure 4-57. The combined water flow rates from the pit bottom during the entire modeling period are plotted in Figures 4-58 and 4-59.
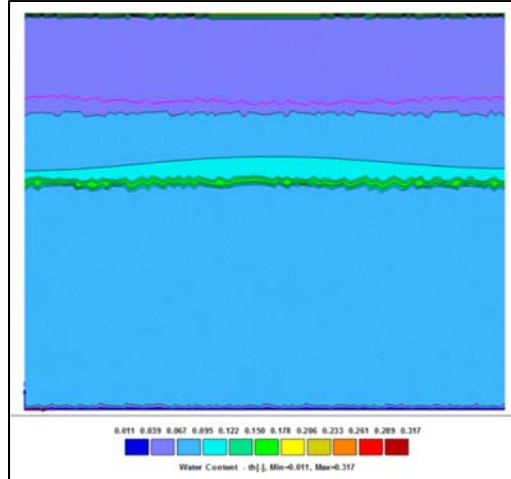
Figure 4-55: Simulated water content distributions for Pit 38 extension at the end of *stage d* (Dec. 31, 3046). A constant recharge rate (or effective infiltration) of 0.1 mm/year is added on the top of the model.
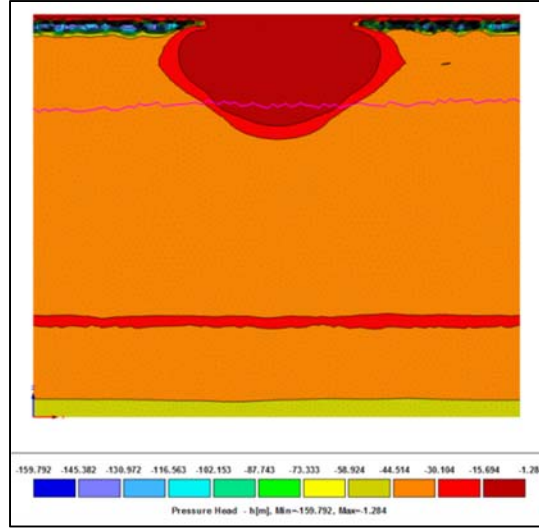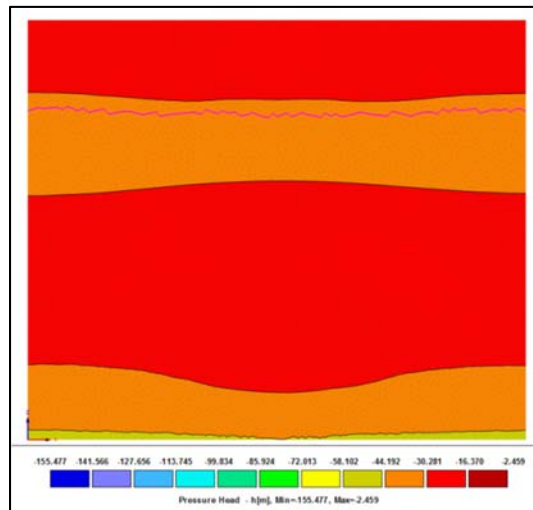

Figure 4-56: Simulated pressure head (m) distributions for Pit 38 extension at the end of *stage d* (Dec. 31, 3046).). A constant recharge rate (or effective infiltration) of 0.1 mm/year is added on the top of the model.
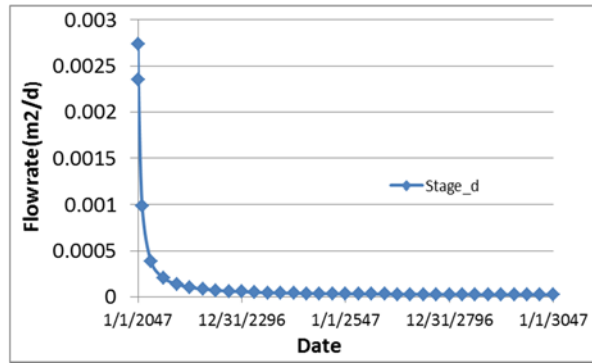
Figure 4-57: Computed water flow rates from the bottom of the Pit 38 extension during *stage d*.
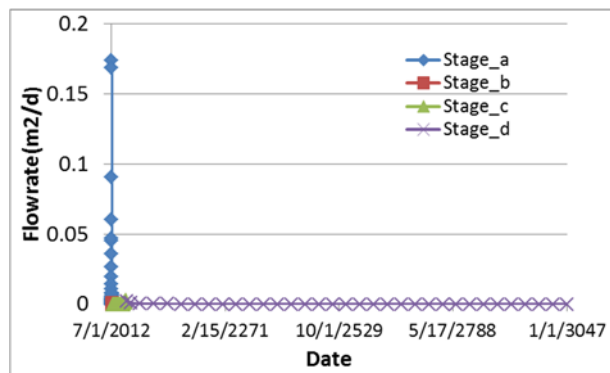
Figure 4-58: Computed water flow rates from the bottom of the Pit 38 extension during the whole modeling period (*stage a* to *stage d*).
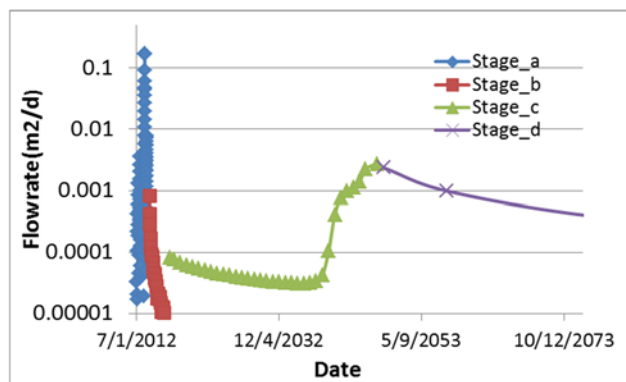
Figure 4-59: Computed water flow rates from the bottom of the Pit 38 extension from *stage a* to early *stage d* using a log scale.

5.0 Summary

This study first introduced the basic theory for modeling water flow in the variably-saturated media with the software HYDRUS. Then, we used three sets of existing monitoring data to conduct flow model validation. Finally, we presented detailed two-dimensional infiltration models under various scenarios for Pit 37, Pit 38 East, Pit 38 West, and the Pit 38 Extension, and we compared the results among different scenarios. The results indicate that different initial saturations (10%, 20% and 33%) assumed for the wastes layers impact water flow rates across the bottoms of the pits but that the water flow rates become more similar with time after waste emplacement. The contaminant control water (dust suppression plus decontamination water) has a large impact on the water flow rates across the bottoms of the pits in a short term (within 2 years) while the large rainfall event in September of 2013 has a much larger impact on the flow rates across the pit bottoms. The computed flow rates after the large rainfall event increased by about two times and lasted for more than 5 years. The impacts from contaminant control water and the 2013 rainfall event decreased with time, and once the pits are assumed to be covered the impacts disappeared. The transient water flow rates calculated with the 2D HYDRUS model are used as input to groundwater flow and transport simulations using FEHM (Pawar et al., 2018).

6.0 References

Birdsell, K.H., A.V. Wolfsberg, D. Hollis, T.A. Cherry, and K.M. Bower. (2000). Groundwater flow and radionuclide transport calcultions for performance assessment of a low-level waste site. *J. Contam. Hydrol*. 46:99–129.

Broxton, D.E., and D.T. Vaniman. (2005). Geologic framework of a groundwater system on the margin of a rift basin, Pajarito Plateau, north-central New Mexico. Available at www.vadosezonejournal.org. *Vadose Zone J*. 4:522–550.

Dai Z, Samper J, Wolfsberg A and Levitt D (2008). Identification of relative conductivity models for water flow and solute transport in unsaturated compacted bentonite, *Physics and Chemistry of the Earth,* 33, S177-S185. doi:10.1016/j.pce.2008.10.012.

Dai, Z. and J. Samper, (2004). Inverse problem of multicomponent reactive chemical transport in porous media: Formulation and applications, *Water Resour. Res.* 40, W074071-W0740718, doi:10.1029/2004WR003248.

Feddes R A, Bresler E and Neuman S P (1974). Field test of a modified numerical model for water uptake by root systems, *Water Resour. Res., 10*(6). 1199-1206.

French, S.B., D. Levitt, P. Stauffer, K. Birdsell, R. Shuman, (2013). Special Analysis 2012-007: Impacts of Water Usage in Pits 37 and 38 at Technical Area 54, Area G, UDQE-1207, Los Alamos National Laboratory, March 2013.

Levitt, D.G., K. Birdsell, T. L. Jennings, and S.B. French (2015). Moisture Monitoring at Area G, Technical Area 54, Los Alamos National Laboratory, June 2015, p98.

Levitt, D.G., (2013). H2D Simulations of Pit 37 & Pit 38 Decon Water for a Special Analysis (Rev2), Internal Report For LANL, Los Alamos, New Mexico.

Levitt, D.G., (2011). *Modeling the Movement of Transient Moisture through DisposalUnits at Los Alamos National Laboratory Technical Area 54, Area G,* Los Alamos National Laboratory Report LA-UR-11-05424, Los Alamos, New Mexico.

Levitt, D.G., (2008). *Modeling of an Evapotranspiration Cover for the Groundwater Pathway at Los Alamos National Laboratory Technical Area 54, Area G,* Los Alamos National Laboratory Report LA-UR-08-5468, Los Alamos, New Mexico. August.

Loaiza, D. and E. Vold, (1995). *Moisture Profiles Measured in Subsurface Monitor Holes at the Los Alamos LLRW Disposal Site*, Los Alamos National Laboratory Report LA-UR-95-1922, Los Alamos, New Mexico.

McLin, S.G., B.D. Newman, and D.E. Broxton, (2005). Vadose zone characterization and monitoring beneath waste disposal pits using horizontal boreholes. *Vadose Zone J.* 4:774-788.

Pawar, R.J., S. Chu, A.A. Atchley, K.H. Birdsell, and P.H. Stauffer (2018). Groundwater Modeling and Predictions of C-14 Transport from Pit 38 at TA-54, Area G, Los Alamos National Laboratory Report LA-UR-18-23491.

Šimůnek J, van Genuchten M Th and Šejna M (2008) Development and applications of the HYDRUS and STANMOD software packages and related codes, *Vadose Zone J.*, 7(2). 587-600. doi:10.2136/vzj2007.0077

Šimůnek J and Hopmans J W (2009) Modeling compensated root water and nutrient uptake, *Ecological Modeling*, *220*(4). 505-521.

Šimůnek J, van Genuchten M Th and Šejna M (2011) The HYDRUS Software Package for Simulating Two- and Three-Dimensional Movement of Water, Heat, and Multiple Solutes in Variably-Saturated Media, Technical Manual, Version 2.0, PC Progress, Prague, Czech Republic, pp. 258.

Stauffer, P.H., H.S. Viswanathan, B.A. Robinson, C.W. Gable, G.L. Cole, D.E. Broxton, E.P. Springer, and T.G. Schofield, (2005). Groundwater Pathway Model for the Los Alamos National Laboratory Technical Area 54, Material Disposal Area G, Los Alamos National Laboratory Report LA-UR-05-7393, September.

van Genuchten M. Th (1980) A closed-form equation for predicting the hydraulic conductivity of unsaturated soils, *Soil Sci. Soc. Am. J., 44*, 892-898.

van Genuchten M Th (1987) A numerical model for water and solute movement in and below the root zone. *Research Report No 121*, U.S. Salinity laboratory, USDA, ARS, Riverside, California.

Zyvoloski, G.A., Robinson, B.A., Dash, Z.V. and Trease, L.L. Summary of the Models and Methods for the (FEHM) Application -- A Finite-Element Heat- and Mass-Transfer Code. LA-13306-MS, Los Alamos National Laboratory, Los Alamos, New Mexico, (2011).

Appendix A: 1000-Year Stochastic Weather Simulation for MDA G
Author: Brent Newman

It is necessary to generate long-term records of meteorological variables (e.g., temperature and precipitation) to help drive hydrological and other processes models used as part of the performance assessment given the need to conduct long-term simulations of MDA G site performance. The existing meteorological records for MDA G in the Los Alamos area do not extend over the 1000-year timeframe needed to make long-term simulations. However, it is possible to generate a 1000-year time series of meteorological variables using a stochastic weather generator based on existing data. Weather generators are now broadly used as part of decision support systems in hydrology, agriculture, and environmental management (Semenov et al., 1998; Semenov et al., 2008). The stochastic weather generation process first includes a detailed statistical characterization of the existing daily meteorological record (e.g., temperature and precipitation). Next, the generator uses the statistical information to calculate synthetic daily meteorological time series for the time period of interest (in this case 1000 years) based on a random number seed. This step is the stochastic aspect of the process, and the resulting time series will have the same statistical properties as the original data. Changing the random number generates a different set of time series, but these series have similar statistical properties as the original data.

In short, the stochastic weather time series represents the local meteorological conditions and their typical variability over time. It is important to note that the resulting series is in no way a prediction of what the weather will be like on some future day. It only represents current broad-scale climate conditions, and this is sufficient for modeling future MDA G performance. The simulated data also assume that current climate characteristics are stationary over the simulation period. In other words, climate change is not included. However, the weather generator used (discussed below) is capable of generating synthetic time series for different climate change conditions including Intergovernmental Panel on Climate Change scenarios.

Input data for the weather generation code was derived from daily weather data from the TA-54 and White Rock weather stations available through (http://weather.lanl.gov/data_request.asp). Data downloaded included daily minimum and maximum temperatures, total daily precipitation,

and solar radiation (note that observed or simulated radiation data are not reported because these data were not used for any MDA G analyses). For the TA-54 station, data were available from 1992-2014. Because this weather station is at TA-54, it is an ideal source of data. The White Rock station data are available from 1965 (first complete year) through 1992, when the TA-54 station came on-line. Post 1992 data for the White Rock station actually come from TA-54 when the data are downloaded through the LANL meteorological site. Given the close proximity of the White Rock station (near the fire station) to MDA G, it was advantageous to use both stations to lengthen the meteorological time series. Having longer records is important for statistically based weather generators, and particularly for semiarid locations which have substantial variability.

Meteorological records typically have missing data for various reasons. For these simulations, data gaps were filled with results from other nearby stations. Prior to 1987, missing values were filled with observations from the Los Alamos station (closest station with data going back into the 1960's). After 1987, missing data were filled using data from the TA-49 station because this station has weather conditions more similar to TA-54. Missing values only accounted for 1.3 to 1.9 percent of the temperature and precipitation time series, so the effects of any differences between the other sites and TA-54 should be small and not affect the simulations substantially.

There are quite a few different weather simulators currently available. The code used here, LARS-WG (http://www.rothamsted.ac.uk/mas-models/larswg/download.php) was selected for the following reasons: 1) LARS-WG has been well documented for site specific weather generation under many different climate conditions/locations (Semenov et al. 1998; Semenov et al. 2008; 2) LARS-WG uses a semi-empirical distribution approach (Rackso et al., 1991) that is more flexible than simple standard distributions used by codes such as WGEN (Richardson and Wright, 1984) and results in better matches to observed data (Semenov et al. 1998); 3) LARS-WG also has better capability to simulate wet or dry periods (e.g., droughts) than WGEN and related codes; 4) LARS-WG provides an extensive set of statistical tools to evaluate how well the simulated time series represents the observed data; and 5) LARS-WG has modules for simulating time series related to climate change scenarios, which may be useful for future MDA G work.

For the current MDA G simulations, the 1965-2014 daily time series described above was used. LARS-WG was used to conduct the initial statistical characterization of the observed time series and then used to generate a 1000-year simulated time series for MDA G. The evaluation statistics included with LARS-WG were also analyzed to assess the quality of the simulation. The LARS-WG manual suggests using a *p* value threshold of 0.1 to evaluate for significant differences between the observed and synthetic time series. For precipitation, Kolmogorov-Smirnov tests for seasonal wet/dry period durations and daily rain distributions by month showed no significant differences between the observed and synthetic series. Monthly means and standard deviations were also not significantly different using T- and F-tests, and there was no significant difference for monthly means related to bias detection. The lack of significant differences indicates that the synthetic precipitation time series should be a good representation of conditions at MDA G.

Kolmogorov-Smirnov comparisons of observed versus synthetic data for minimum and maximum temperatures were also not significantly different for daily distributions. However, there were multiple instances where monthly means and standard deviations were significantly different for temperatures using T- and F-tests. Bias tests for monthly mean minimum and maximum temperatures did not show any significant differences. Tests of seasonal cold spell distributions did not show any significant differences, but there were significant differences for heat spells in March/April/May and June/July/August. These kinds of significant differences with monthly temperatures and heat spells are not uncommon in weather generators because the observed data have significant temporal correlation, and the synthetic data vary more randomly because of the simple autocorrelation structure in the models (Semenov et al., 2008). In addition, even though the observed time series is 49-years long, it probably still does not fully capture the variability of the semiarid climate. For example, the temperatures of recent drought periods are probably not as well characterized in the statistical model as say a 100-year observational period might provide. Overall, the synthetic temperatures, while not perfect, appear to be reasonable approximations of conditions at MDA G for the purposes of the performance assessment. It is unlikely that significant improvements can be made without either substantially more observed data, or the development of new approaches to simulating temperature time series. The fact that precipitation is well simulated is also a strong reason for accepting the synthetic 1000-year time series for use as input into hydrological models for the MDA G performance assessment.

References

Racsko, P., Szeidl, L., Semenov, M., 1991. A serial approach to local stochastic weather models. Ecological modelling, 57(1): 27-41.

Richardson, C.W., Wright, D.A., 1984. WGEN: A model for generating daily weather variables. US Department of Agriculture, Agricultural Research Service Washington, DC, USA.

Semenov, M.A., 2008. Simulation of extreme weather events by a stochastic weather generator. Climate Research, 35(3): 203.

Semenov, M.A., Brooks, R.J., Barrow, E.M., Richardson, C.W., 1998. Comparison of the WGEN and LARS-WG stochastic weather generators for diverse climates. Climate research, 10(2): 95-107.